Engineering an Exo70 integrated domain of a barley NLR for improved blast resistance

Indira Saado[1], Helen J. Brabham[2,3], Josh W. Bennett[1], Anson Ho Ching Lam[4], Inmaculada Hernández-Pinzón[2], Matthew J. Moscou[2,5], Juan Carlos De la Concepcion[1,2,6*], Mark J. Banfield[1*]

Address:

[1] *Department of Biochemistry and Metabolism, John Innes Centre, Norwich Research Park, Norwich, NR4 7UH, UK*

[2] *The Sainsbury Laboratory, University of East Anglia, Norwich Research Park, Norwich, NR4 7UH, UK*

[3] *2Blades, Evanston, IL 60201, USA*

[4] *Department of Cell and Developmental Biology, John Innes Centre, Norwich Research Park, Norwich, NR4 7UH UK*

[5] *USDA-ARS Cereal Disease Laboratory, University of Minnesota, 1551 Lindig Street, Saint Paul, Minnesota, 55108 USA*

[6] *Gregor Mendel Institute of Molecular Plant Biology, Austrian Academy of Sciences, Vienna, 1030, Austria*

[*]Corresponding authors: Juan Carlos De la Concepcion (juan.concepcion@gmi.oeaw.ac.at), Mark J. Banfield (mark.banfield@jic.ac.uk)

ORCID IDs:

Indira Saado: 0000-0002-3462-0983

Helen Brabham: 0000-0001-7132-5011

Josh W. Bennett: 0000-0001-8576-7195

Anson Ho Ching Lam: 0000-0001-7805-2132

Inmaculada Hernández-Pinzón: 0000-0003-3711-2893

Matthew J. Moscou: 0000-0003-2098-6818

Juan Carlos De la Concepcion: 0000-0002-7642-8375

Mark J. Banfield: 0000-0001-8921-3835

Summary

Intracellular immune receptors protect plants from microbial invasion by detecting and responding to pathogen-derived effector molecules, often triggering cell death responses. However, pathogen effectors can evolve to avoid immune recognition, resulting in devastating diseases that threaten global agriculture. Here, we show that an integrated Exo70 domain from the barley NLR RGH2 can interact with both the rice blast pathogen effector AVR-Pii and a closely related wheat blast variant. We used structure-led engineering to develop RGH2^{+} that shows increased binding affinity towards AVR-Pii variants and increased cell death responses on heterologous expression in *Nicotiana benthamiana*. Infection assays in transgenic barley lines carrying RGH2^{+} with the paired NLR RGH3 indicate a reduced susceptibility to blast strains expressing AVR-Pii variants. These results demonstrate the potential of engineering NLR receptors as an effective strategy for improving resistance towards one of the most destructive diseases affecting cereal production.

Introduction

Plants are continuously threatened by pathogens and rely on an innate immune system for defence. One critical component of this immune system is the recognition of virulence proteins (effectors) that are delivered from pathogens to manipulate host cells for the benefit of the invading organism. *Magnaporthe oryzae* is a devastating ascomycete fungus that infects cereal crops, including rice, wheat, barley, and other grasses, causing blast disease[1,2]. Since the pathogen's host jump to wheat in South America in the 1980s[3,4], and recent spread to Asia and Africa[5], wheat blast disease (caused by *M. oryzae* pathotype *Triticum*) has emerged as major pandemic threat to agriculture. *M. oryzae* deploys a diverse set of effectors during colonization, targeting key plant processes to promote infection. Despite their essential roles in infection, the function of only a limited number of *M. oryzae* effectors has been fully characterized.

Pathogen effectors can be sensed by intracellular nucleotide-binding leucine-rich repeat (NLR) receptors, triggering immune responses that often result in localised cell death, limiting the spread of infection. As such, engineering NLRs for novel recognition profiles can unlock promising strategies for improved disease resistance[6–9]. Canonical NLRs comprise an N-terminal signalling domain, a central nucleotide-binding adaptor NB-ARC switch domain, and a C-terminal leucine-rich repeat (LRR) domain involved in intramolecular molecular contacts and pathogen effector recognition[10]. While some NLRs function alone to both sense and respond to effectors (singleton NLRs), others function in pairs, with a sensor NLR to recognize the effector, directly or indirectly, and a helper NLR required for immune response execution. Such pairs can be co-located in plant genomes including in head-to-head orientations with shared promoters, or function as part of distributed genetic networks[11,12].

To date, two co-located paired NLR systems have been extensively studied in rice: Pik-1/Pik-2[13,14] and RGA5/4[15,16]. Both sensor NLRs, Pik-1 and RGA5, contain non-canonical integrated heavy metal-associated (HMA) domains to bait specific effectors from *M. oryzae*[17–20]. The sensor NLR Pik-1 contains a HMA domain positioned between the CC and NB-ARC domains, and with the helper NLR Pik-2 cooperatively triggers immunity against the blast pathogen effector AVR-Pik[13,14,18,21,22]. The Pik/AVR-Pik system has emerged as a model for how receptor engineering can lead to novel immune outcomes[6–8,19,20,23,24]. By contrast, the sensor NLR RGA5 has an HMA domain

at the C-terminus (after the LRR) and baits the blast pathogen effectors AVR-Pia and AVR1-CO39[25]. Activation of immunity requires the helper NLR RGA4[26,27]. This NLR pair has also been leveraged for engineering immunity to expand effector recognition profiles[28].

In addition to direct effector recognition, paired NLRs can indirectly recognise pathogen effectors[29–31]. For example, the unconventional RIN4 (RPM1-Interacting Protein 4)-like NOI (nitrate induced) domain of the rice sensor NLR Pii-2 monitors the status of host OsExo70-F2/3 proteins targeted by the rice blast Zinc-finger fold (ZiF) effector AVR-Pii[29–32]. Canonical Exo70 proteins are part of the exocyst, a conserved protein complex essential for tethering secretory vesicles to membranes[33,34].However, in plants, the Exo70 family has dramatically expanded[35] and acquired novel functions independent from the exocyst[33,36–38], including plant defence[39–43], making this protein a target for pathogen effectors[44]. Integrated domains in NLRs, such as HMAs, are likely derived from the host virulence-associated targets of effectors, repurposed for effector perception[45]. Recently, a head-to-head NLR pair from the barley cultivar Baronesse was identified comprising the sensor NLR RGH2, containing a C-terminal Exo70 integrated domain, and its helper NLR RGH3[46]. The integration of an Exo70 domain in RGH2[47] suggests a potential role in immunity by serving as an integrated domain to bait effectors for recognition.

In this study, we show that the Exo70 integrated domain of the barley sensor NLR RGH2 can interact with the rice blast effector AVR-Pii and a closely related wheat blast variant in vitro and in vivo. On co-expression with the helper NLR RGH3, the RGH2/RGH3 pair elicits limited cell death to the AVR-Pii variants in *N. benthamiana*. Based on the crystal structure of the OsExo70F2/AVR-Pii complex[29], we engineered a new immune receptor, RGH2^{+}, that showed enhanced binding affinity towards AVR-Pii variants, leading to improved cell death responses on co-expression with RGH3 in *N. benthamiana*. In transgenic barley, RGH2^{+}/RGH3 confers a reduction in disease severity compared to the wild-type RGH2/RGH3 when infected with *M. oryzae* expressing AVR-Pii. These findings establish the RGH2/RGH3 NLR pair as a platform for engineering enhanced effector response profiles and highlights new opportunities for protecting cereal crops from blast disease.

Results

Multiple Exo70 domains are integrated in NLRs across the Poales order

Previous work established that NLRs from diverse plant species carry integrated domains[48,49]. We sought to identify NLRs with integrated Exo70 domains to understand their source and assess their use as scaffolds for NLR engineering. To enrich the set of NLRs for analysis, we performed de novo transcriptome assembly of publicly available RNAseq data for 102 Poales species including a total of 292 accessions (Fig. 1A). Domain annotation identified 184,775 NB-ARC domain containing proteins. Within this set of NB-ARC containing proteins, 82 were found to also have an Exo70 domain. Comparative analysis of these integrated Exo70 domains found that the 82 putative integrated Exo70 domains are derived from eight unique fusion events. Among these, six domains were found to be of sufficient length for phylogenetic analysis with grass Exo70 domains[43]. Maximum likelihood phylogenetic analysis using Exo70 from eight grass species found the six integrated Exo70 domains were placed in either the Exo70F or Exo70FX clades (Fig. 1B). The most prevalent integration is RGH2 that carries a C-terminal fusion with Exo70F1, which was originally identified at the *Mla* locus in the barley (*Hordeum vulgare*) accession Baronesse. This integration event was found in seven species within Triticeae and Poeae tribes[47]. In barley, a second NLR, Hvu23934, was found with integration of Exo70FX2 in three Triticeae species (*Aegilops sharonensis*, *Ae. speltoides*, and *H. vulgare*). The remaining four integrated domains are found in single species: *Arundinella pubescens* (Panicoideae; Apu26724; NLR-Exo70F4), *A. pubescens* (Panicoideae; Apu28443; NLR-Exo70F2), *Holcus lanatus* (Pooideae; Hla80948; NLR-Exo70FX2), and *Juncus effusus* (Juncaceae; Jef9120; NLR-Exo70F) (Supplementary Fig. S1). These integrated domains (excluding Apu26724) were taken forward for further analysis.

Rice blast AVR-Pii and the wheat blast variant bind the barley RGH2-Exo70 integrated domain in yeast

As some ZiF effectors, including AVR-Pii, bind rice Exo70s from clade F, we tested whether Exo70 integrated domains could bind ZiF effectors from rice and wheat-infecting blast isolates of *M. oryzae* in pairwise yeast two-hybrid (Y2H) assays. For this we cloned the Exo70 integrated domains from the NLRs RGH2, Hvu23924, Hla80948, Jef9120, and Apu28443 and tested their binding to representatives of each ZiF effector clade from rice and wheat-infecting blast isolates. These assays revealed

143 that ZiF effectors from tribe VIII, from both rice blast (ZiF_VIIId, hereafter AVR-Pii^{Rb})
144 and wheat blast (ZiF_VIIIc, hereafter AVR-Pii^{Wb}) isolates bound RGH2-Exo70, as did
145 tribe IX member ZiF_IXj (Fig. 2A). We did not observe interactions between other NLR
146 Exo70 integrated domains and any ZiF effectors tested (Supplementary Fig. S3A,
147 S4A, S5A). We observed yeast growth with Apu28443-Exo70 in the presence of all
148 tested ZiF effectors, likely indicating autoactivity (Supplementary Fig. S6A). Therefore,
149 we did not investigate it further in this study. Protein accumulation was assessed by
150 western blot (Supplementary Fig. S2A, S3B, S4B, S5B, S6B).

151 The crystal structure of AVR-Pii^{Rb} in complex with OsExo70F2[29] identified Phe-65 as
152 a key interacting residue from the effector, and a Phe65Glu mutation in AVR-Pii^{Rb}
153 abolished the interaction with OsExo70F3[29]. AVR-Pii^{Wb} is predicted to adopt the
154 conserved ZiF structural fold, as observed for AVR-Pii^{Rb} (Supplementary Fig. S7A, B),
155 and binds to OsExo70F3[32]. To test whether AVR-Pii^{Rb} and AVR-Pii^{Wb} interact with the
156 RGH2-Exo70 integrated domain via a similar interface, we tested the binding of both
157 AVR-Pii^{Rb} and AVR-Pii^{Wb} Phe to Glu mutants to RGH2-Exo70 by Y2H. This assay
158 revealed that these mutants do not bind RGH2-Exo70 (Fig. 2B). Protein accumulation
159 was assessed by western blot (Supplementary Fig. S2B).

160 AVR-Pii^{Rb} and AVR-Pii^{Wb} bind the barley RGH2-Exo70 integrated domain 161 in planta

162 To further validate the interaction between AVR-Pii^{Rb} or AVR-Pii^{Wb} with RGH2-Exo70,
163 we used co-immunoprecipitation (co-IP) assays in *N. benthamiana*. RGH2-Exo70-
164 FLAG was co-expressed with GFP-AVR-Pii^{Rb}, GFP-AVR-Pii^{Wb} and their respective
165 Phe to Glu mutants. We also co-expressed the effectors with OsExo70F3-FLAG as
166 positive and negative controls, respectively. Following extraction and
167 immunoprecipitation with anti-FLAG beads (to capture Exo70 domains), both
168 effectors, but not their Phe to Glu mutants, were pulled down (Fig. 2C). Interestingly,
169 we observe that the detected levels of AVR-Pii^{Rb} and AVR-Pii^{Wb} in the co-IPs are higher
170 with OsExo70F3 compared to the RGH2-Exo70, suggestive of a stronger association.

171 AVR-Pii^{Rb} and AVR-Pii^{Wb} bind more weakly to RGH2-Exo70 than 172 OsExo70F3 in vitro

173 To further investigate the binding of AVR-Pii^{Rb} and AVR-Pii^{Wb} to RGH2-Exo70 we
174 produced and purified these proteins from *Escherichia coli*. We then performed
175 isothermal titration calorimetry (ITC) assays to assess the binding strength between
176 effectors and the RGH2-Exo70 domain. Previous results show that AVR-Pii^{Rb} binds to
177 OsExo70F3 in the nano-molar range (K_D of 1.0x10^{-10} M)[29]. RGH2-Exo70 binds AVR-
178 Pii^{Rb} and AVR-Pii^{Wb} in the micro-molar range (K_Ds of 1.5x10^{-5} M and 6.7x10^{-6} M
179 respectively), showing that AVR-Pii^{Rb} binds OsExo70F3 more tightly than RGH2-
180 Exo70 in vitro (Supplementary Fig. S2D), and AVR-Pii^{Wb} binds RGH2-Exo70 in the
181 same range as AVR-Pii^{Rb}. No binding was observed with the effector mutants AVR-
182 Pii^{RbF65E} or AVR-Pii^{WbF66E} with OsExo70F3 or RGH2-Exo70 (Fig. 2D)[29].

183 Taken together, the results from Y2H, co-IP, and ITC show that while AVR-Pii^{Rb} and
184 AVR-Pii^{Wb} bind to RGH2-Exo70, this interaction is not as robust as to OsExo70F3.
185 This suggests that engineering RGH2-Exo70 for improved effector binding could
186 enhance effector perception and immunity-related signalling by this receptor.

187 An engineered RGH2$^+$ NLR shows higher binding affinity towards AVR-
188 Pii^{Rb} and AVR-Pii^{Wb}

189 We hypothesised that engineering a new binding interface to RGH2-Exo70, mimicking
190 OsExo70F3, could improve interaction strength. Guided by the structure of the
191 OsExo70F2/AVR-Pii complex[29], we generated a modified version of RGH2, RGH2$^+$,
192 by introducing three mutations, Ala1378Val, Ile1379Leu, and Leu1396Met (Fig. 3A).
193 AlphaFold3[50] predictions of the RGH2-Exo70 and RGH2$^+$-Exo70 structures indicate a
194 conserved fold with OsExo70F2 (Fig. 3B).

195 To assess the binding capabilities of the RGH2$^+$-Exo70 domain towards AVR-Pii^{Rb} and
196 AVR-Pii^{Wb} we first used the Y2H assay. This showed that the engineered NLR retained
197 binding to these two effectors, and confirmed the same surface of the effector is
198 required for binding as the respective Phe to Glu mutations prevented interaction (Fig.
199 3C). Protein accumulation was assessed by western blot (Supplementary Fig. S8).

200 To compare interactions between AVR-Pii^{Rb} and AVR-Pii^{Wb} with RGH2 or RGH2$^+$ in
201 plant cells, we first used co-IP. FLAG-tagged full-length RGH2 and RGH2$^+$
202 immunoprecipitated GFP-tagged AVR-Pii^{Rb} and AVR-Pii^{Wb}, but not the Phe to Glu
203 mutants of each effector (Fig. 3D). Additional negative controls, including a double

204 mutant Tyr to Ala, Phe to Glu, and a ZiF effector from a tribe that does not interact
205 with Exo70s (ZiF_IIb), were not immunoprecipitated by RGH2 or RGH2^{+}
206 (Supplementary Fig. S9). Secondly, we used the split GAL4 RUBY assay that allows
207 quantification of protein-protein interactions in plant cells through the production of
208 betalain[51]. Agrobacterium strains carrying OsExo70F3-Gal4-BD, RGH2-Exo70-Gal4-
209 BD, or RGH2^{+}-Exo70-Gal4-BD were co-infiltrated with constructs containing VP16-
210 tagged AVR-Pii^{Rb} or AVR-Pii^{Wb} or their Phe to Glu mutants (all constructs under the
211 control of the *35Sprom*). Betalain production was observed 3 days post-infiltration (dpi)
212 (Supplementary Fig. S10A, S11A). Intriguingly, significantly higher betalain production
213 was observed in RGH2^{+}-Exo70 leaves compared to RGH2-Exo70 with AVR-Pii^{Rb}.
214 However, with VP16-AVR-Pii^{Wb}, levels of betalain production accumulated at similar
215 levels. Low betalain production was observed with the VP16-tagged effector mutants
216 in combination with Exo70 constructs. To determine whether lower effector expression
217 in *N. benthamiana* leaves could allow distinction between RGH2-Exo70 and RGH2^{+}-
218 Exo70 responses to AVR-Pii^{Wb} in this assay, we generated AVR-Pii expression
219 constructs under the control of the *MAS* promoter. Notably, overall betalain production
220 was lower compared to the *35Sprom* assays. However, in these conditions, we
221 observed significant differences between RGH2-Exo70 and RGH2^{+}-Exo70 with both
222 AVR-Pii^{Rb} and AVR-Pii^{Wb} (Fig. 4A, B). Protein accumulation for all constructs was
223 assessed by western blot (Supplementary Fig. S10B, S11B).

224 RGH2^{+}-Exo70 binds AVR-Pii^{Rb} and AVR-Pii^{Wb} more tightly compared to 225 wild-type in vitro

226 To extend the in vivo analysis, we purified RGH2^{+}-Exo70 from *E. coli* and tested
227 binding to AVR-Pii^{Rb} and AVR-Pii^{Wb} by ITC. Consistent with the RUBY assay, the
228 binding affinity of RGH2^{+}-Exo70 to AVR-Pii^{Rb} and AVR-Pii^{Wb} was increased compared
229 to RGH2-Exo70, with a dissociation constant (K_D) of 3.12×10^{-6} M and 1.06×10^{-6} M,
230 respectively (Fig. 4C). No binding to RGH2^{+}-Exo70 was observed with AVR-Pii^{RbF65E}
231 or AVR-Pii^{WbF66E} (Fig. 4C). These in vitro experiments confirmed tighter binding of
232 RGH2^{+}-Exo70 towards AVR-Pii^{Rb} and AVR-Pii^{Wb} compared to the wild type RGH2-
233 Exo70.

234 RGH2^{+}/RGH3 enhanced cell death responses to AVR-Pii^{Rb} and AVR-Pii^{Wb} 235 in *N. benthamiana*

236 We hypothesised that increased effector binding to RGH2^{+}-Exo70 may translate into
237 improved immune responses in plants compared to RGH2. To test this, we first co-
238 expressed RGH2 and RGH3 in *N. benthamiana* alone to assess potential autoactivity,
239 and with AVR-Pii^{Rb} or AVR-Pii^{Wb} to observe effector-dependent cell death. Imaging
240 leaves three days post infiltration revealed that no macroscopic cell death was
241 observed for RGH2/RGH3 alone, or when co-expressed with GFP or with effector Phe
242 to Glu mutants (Fig. 5A, 5B). However, cell death was observed under both white light
243 and UV light on co-expression of RGH2/RGH3 and either of AVR-Pii^{Rb} or AVR-Pii^{Wb}
244 (Fig. 5A, 5B). In parallel, to test the impact of RGH2^{+} on cell death, we co-expressed
245 this NLR with RGH3, both with and without effectors. Again, we did not observe
246 autoactivity, or cell death with negative controls. Intriguingly, we observed qualitatively
247 stronger cell death in leaf spots infiltrated with RGH2^{+} compared to RGH2, and the
248 cell death was stronger with AVR-Pii^{Wb} over AVR-Pii^{Rb} (Fig. 5A, 5B). To quantify the
249 cell death on expression of NLRs and effectors in *N. benthamiana*, we measured
250 electrolyte leakage from leaf disks at 4, 24, and 48 hours post-infiltration (Fig. 5C,
251 S12A, B). Here, we observed significant increases in conductivity from samples of
252 RGH2^{+}/RGH3-infiltrated tissue with AVR-Pii^{Wb} over AVR-Pii^{Rb} compared to
253 RGH2/RGH3. RGH2/RGH3 or RGH2^{+}/RGH3 with AVR-Pii^{F65E} displayed minimal
254 change in conductivity compared with RGH2/RGH3 and RGH2^{+}/RGH3 alone (Fig. 5C,
255 Supplementary Fig. S12A, B). We also observed higher levels of conductivity in
256 samples with AVR-Pii^{Wb} compared to AVR-Pii^{Rb}, in agreement with the macroscopic
257 cell death observations. Protein accumulation was assessed by western blot for all *N.*
258 *benthamiana* cell death experiments (Fig. 5D, E). Collectively, these data demonstrate
259 that RGH2^{+}/RGH3 exhibits a stronger cell death response towards the effectors
260 compared to RGH2/RGH3 in *N. benthamiana*, and that AVR-Pii^{Wb} elicits a stronger
261 response than AVR-Pii^{Rb}.

262 Enhanced recognition of AVR-Pii^{Wb} by RGH2^{+}/RGH3 in transgenic barley 263 plants

264 We hypothesised that the increase in cell death response of RGH2^{+}/RGH3 to effectors
265 compared with RGH2/RGH3 in *N. benthamiana*, could confer improved disease
266 resistance in barley to pathogens encoding these effectors. For this, we focussed on
267 AVR-Pii^{Wb} due to the need to explore novel resistances against wheat blast[52].

The wild-type RGH2/RGH3 was previously cloned with the native promoter and terminator and transformed into the barley cultivar Golden Promise[46]. The RGH2/RGH3 genomic transformation construct was edited using site-directed mutagenesis to covert the integrated Exo70 binding site into RGH2+ and was transformed into the barley cultivar Golden Promise using Agrobacterium-mediated transformation.

RGH2^{+}/RGH3 and RGH2/RGH3 transgenic T1 families were tested for recognition of AVR-Pii^{Wb} by inoculation with *M. oryzae* isolate Guy11 (lacking AVR-Pii) transformed with AVR-Pii^{Wb} (Golden Promise is susceptible to Guy11). Spray inoculation on detached leaves was used to assess phenotypes, which were scored on a macroscopic 0-4 scale for disease severity[53](Fig. 6A, C). For RGH2/RGH3 transgenics, four independent T1 families were screened with 84, 72, and 82 individuals screened across experimental replicates. For RGH2^{+}/RGH3 transgenics, four independent T1 families were screened with 119, 91, and 93 individuals across replicates. A total of 88, 117, and 131 individuals of the susceptible Golden Promise transgenic background were screened across replicates (Figure 6B).

To evaluate the effect of RGH2^{+}/RGH3 and RGH2/RGH3 on disease severity, we used a cumulative link mixed model fitted with the Laplace approximation to assess the ordinal infection scores. The model included the accession (RGH2^{+}/RGH3, RGH2/RGH3, and Golden Promise) as a fixed effect, with random effects of experimental replicate, independent transgenic families, and the interaction between replicate and transgenic family. For the random effects, variability is observed across replicates ($\sigma^2 = 0.83$, SD = 0.91), independent families perform slightly differently across replicates ($\sigma^2 = 0.37$, SD = 0.61), and plants within the same independent family show minimal variation ($\sigma^2 = 0.01$, SD = 0.10). A significant difference was observed between RGH2^{+}/RGH3 transgenics compared to the Golden Promise control ($\beta = -1.90$, SE = 0.44, $z = -4.28$, $p < 0.0001$). By contrast, RGH2/RGH3 transgenic lines showed no significant difference from the control ($\beta = -0.20$, SE = 0.44, $z = -0.46$, $p = 0.648$), suggesting that RGH2/RGH3 alone does not confer reduced disease severity under our experimental conditions (Fig. 6A, B).

Further, post-hoc pairwise comparisons of estimated marginal means using Tukey's HSD confirmed these results. RGH2^{+}/RGH3 transgenic lines demonstrated

300 significantly reduced disease severity to Guy11 transformed with AVR-Pii^{Wb} compared
301 to both RGH2/RGH3 transgenic lines (difference = 1.70, SE = 0.32, $p < 0.001$) and
302 Golden Promise (difference = 1.90, SE = 0.44, $p < 0.001$). No significant difference
303 was observed between RGH2/RGH3 and Golden Promise (difference = 0.20, SE =
304 0.44, $p = 0.891$) (Fig. 6A, B). Therefore, engineered RGH2^{+}/RGH3 confers reduced
305 disease severity compared to wild-type RGH2/RGH3.

306

Discussion

NLR immune receptors play a crucial role in protecting plants against pathogens and are a critical component of disease resistance breeding programs in crops. The diverse effector repertoires of pathogens and their ability to adapt to immune systems presents challenges that can limit the effectiveness of NLRs deployed in agriculture. Approaches to address this limitation include engineering NLRs to broaden their recognition spectrum to target conserved effectors across pathogen isolates. Here, we have introduced structure-guided mutations in the effector binding interface of the Exo70 integrated domain of the barley NLR immune receptor RGH2 to enhance binding to rice and wheat blast effectors. Using a combination of in vitro and in vivo experiments, we demonstrate this engineered RGH2^{+} shows higher affinity binding towards rice blast AVR-Pii and the wheat blast variant compared to RGH2, leading to improved immune responses and reduced pathogen virulence in transgenic barley lines.

With the emergence of new disease pandemics, such as wheat blast that threatens yields across Asia and Africa, there is a pressing need for identifying new sources of resistance[54–56]. Screening wild species and landraces for novel resistance traits continues to deliver new genes and germplasm for breeding[57]. Alternative approaches are enabled by advances in understanding the molecular mechanisms of plant immune receptor structure and function. Such knowledge can be deployed through engineering and improved transformation pipelines, alongside ongoing improvements in gene-editing tools.

NLR integrated domains (NLR-IDs) bait pathogen effectors for immune activation in cereals and other plants[14,58–60]. They present opportunities for receptor engineering, to optimise effector recognition ahead of activating conserved downstream mechanisms of NLR-mediated immunity[14,59]. Exo70 integrated domains are under-studied compared to other examples such as HMA and WRKY domains[13,14,16,20,59,60]. The best studied example of NLR-mediated immunity requiring Exo70 proteins is towards the *M. oryzae* effector AVR-Pii. However, in this case the Exo70 protein is guarded by the NLR pair Pii, and not integrated within an immune receptor[30,31]. In plants, Exo70 proteins form an expanded family with increased gene copy number and functional diversification[35,36,38,43] and they are targeted by effectors from diverse

339 pathogens[44]. Our study highlights the potential of engineering NLR integrated Exo70
340 domains to mediate activation of immunity.

341 Our rationale for RGH2-Exo70 engineering was guided by the interface formed in the
342 crystal structure of the OsExo70F2/AVR-Pii complex[29]. The mutations to generate
343 RGH2^{+} resulted in subtle changes to amino acid properties at the interface, including
344 Alanine to Valine (position 1378), Isoleucine to Leucine (position 1379) and Leucine
345 to Methionine (position 1396). We hypothesised these differences could explain the
346 reduced affinities of AVR-Pii^{Rb} and AVR-Pii^{Wb} to RGH2-Exo70 over OsExo70F3, and
347 ultimately improve the binding and response of the RGH2^{+}/RGH3 pair. Subtle changes
348 acquired in effectors through evolution can result in escape from detection by plant
349 immune receptors, potentially reducing their effectiveness in crops. By contrast, we
350 show here that subtle amino acid changes can be harnessed to engineer receptors to
351 boost plant immunity, including to effector families conserved across pathogen
352 isolates. These changes maybe more broadly suitable for targeted gene-editing
353 approaches in agriculture, balanced against larger scale genetic modifications (e.g.
354 domain swapping or full gene transformation). However, while OsExo70F3 binds AVR-
355 Pii^{Rb} with nanomolar affinity, RGH2^{+} binding to AVR-Pii^{Rb} and AVR-Pii^{Wb} remains within
356 the micromolar range. This suggests there may be opportunities, beyond the scope of
357 this study, to further improve effector binding to RGH2 and response to wheat blast
358 expressing AVR-Pii^{Wb}.

359 Effectors form diverse sequence and structural repertoires across different pathogen
360 isolates[61–63]. AVR-Pii^{Rb} and AVR-Pii^{Wb} are both members of tribe VIII of the Zinc-finger
361 (ZiF) effector family[32], sharing 72 % sequence identity. We observed that AVR-Pii^{Rb}
362 and AVR-Pii^{Wb} elicit different levels of RGH2/RGH3 activation, which was even clearer
363 with RGH2^{+}/RGH3. Specifically, AVR-Pii^{Wb} elicited stronger cell death compared to
364 AVR-Pii^{Rb} in *N. benthamiana* assays (Fig. 5A). ZiF effectors from different tribes
365 (including tribe VIII) are prevalent in wheat blast lineages compared to rice blast,
366 where many are either absent or are pseudogenes[32]. While we focussed on
367 engineering the barley NLR RGH2 receptor pair towards AVR-Pii^{Rb} and AVR-Pii^{Wb}
368 here, there are future opportunities to expand responses towards other ZiF family
369 members by exploring surface complementarity between predicted effector structures
370 and the binding sites of Exo70 integrated domains using computational approaches[64].

371 In particular, this includes members from ZiF effector Tribes VII and IX, as these were
372 previously shown to bind OsExo70F3[32].

373 In this study, we aimed to engineer new resistance to effectors from the blast pathogen
374 (specifically wheat blast) and in general broaden our understanding of NLR-mediated
375 resistance mechanisms. Engineering of the NLR RGH2, guided by the binding of rice
376 blast AVR-Pii to OsExo70F2, reduced the disease severity of *M. oryzae* when
377 introduced in transgenic barley. Additional work is required to explore the potential to
378 increase resistance further, possibly through new enhanced receptor-effector binding
379 variants or optimising NLR expression levels.

380 ## Conclusion and outlook

381 Engineering NLR integrated domains is a promising path to expand the effector
382 recognition profile of these plant immune receptors. Previously, the rice NLR pairs Pik
383 (Pik-1/Pik-2) and Pia (RGA4/RGA5), which both contain integrated HMA domains in
384 their sensor NLRs to bait effectors, have been engineered with novel response profiles
385 [19,20,28,65]. Here, we further the concept of NLR integrated domain engineering to the
386 Exo70 domain of the RGH2/RGH3 pair, demonstrating its promise as a scaffold to
387 expand the spectrum of effector recognition specificities.

388 Looking ahead, future directions could involve applying this system to wheat cultivars.
389 Interestingly, RGH2/RGH3 is present in rice, however RGH2 has an integrated
390 thioredoxin domain rather the Exo70[47]. As AVR-Pii has been lost from most *M. oryzae*
391 isolates infecting rice (likely due to deployment of Pii-based resistance in rice) the
392 evolution of different integrated domains in the RGH2/RGH3 architecture supports this
393 chassis as an appropriate target for engineering. Finally, it may be possible to engineer
394 resistance to other pathogens by installing additional diverse Exo70 domains, or other
395 unrelated effector targets.

396 # Method details

397 ## Plasmids and cloning procedures

398 *Escherichia coli* Stellar™ (Takara Bio), SHuffle (Invitrogen) and Rosetta™ (DE3) cells
399 were used for cloning and protein expression. All plasmids were generated by either
400 In-Fusion® cloning (Takara Bio, USA) or the Goldengate system[66] using resources
401 from TSL Synbio. All plasmids are described in **Supplementary Table 1**, enabling full
402 details of constructs used, including epitope tags. The modules used were either
403 amplified by PCR, synthesized as PCR products (Gblocks, GeneWiz) or obtained from
404 TSL SynBio. Restriction enzymes were purchased from New England Biolabs
405 (Ipswich, MA, USA). Primers and their purpose are listed in **Supplementary Table 2**.

406 ## Transcriptome assembly and phylogenetic analysis

407 Publicly available RNAseq data sets for Poales species were identified from NCBI SRA
408 database and *de novo* transcriptome assemblies were generated using Trinity with
409 default parameters (version 2013-11-10). The Poales species phylogenetic tree was
410 generated using the QKbusco pipeline (https://github.com/matthewmoscou/QKbusco)
411 as described in Brabham *et al.,* (2025)[53]. Briefly, open reading frames from assemblies
412 predicted using TransDecoder (v4.1.0). Benchmarking universal single-copy orthologs
413 were identified using BUSCO (v3.0.2) with default parameters and embryophyte_odb9
414 library. Genes identified with BUSCO were used to generate a multiple sequence
415 alignment using QKbusco_merge.py using parameter 'allfragmented'. Codon-based
416 multiple sequence alignment was performed with PRANK (v.170427) using default
417 parameters. Multiple sequence alignments were merged using
418 QKbusco_phylogeny.py with coverage depth of 40% at individual sites. The maximum
419 likelihood phylogenetic tree was generated using RAxML (v8.2.12) with the
420 GTRGAMMA model.
421 InterProScan (v5.27-66.0) using default parameters was used to identify NB-ARC
422 (Pfam PF00027 and PF00931) and Exo70 (Pfam PF03081) domain containing
423 proteins from *de novo* transcriptomes predicted proteins from TransDecoder. Domain
424 boundaries of integrated NLRs were manually curated based on Pfam annotation.
425 Phylogenetic analysis of Exo70 domains was carried out as described by Holden *et*
426 *al.*, (2022)[43]. Briefly, structure-guided multiple sequence alignment was performed with
427 MAFFT software (v7.481) using DASH (Database of Aligned Structural Homologs)

428 with default parameters. Structurally resolved Exo70 structures included *A. thaliana*
429 Exo70A1 (PDB 4RL5), *S. cerevisiae* (yeast) Exo70 (PDB 2B1E and 5YFP), and *Mus*
430 *musculus* (mouse) (PDB 2PFT). The maximum likelihood phylogenetic tree was
431 constructed using RAxML (v8.2.12) with the JTT amino acid substitution model,
432 gamma model of rate heterogeneity, and 1,000 bootstraps. iTOL (Interactive Tree of
433 Life) was used for phylogenetic tree visualization, and *S. cerevisiae* and *M. musculus*
434 Exo70 were used as outgroups.
435

436 **Cell death assay**

437 Four-week-old *N. benthamiana* plants were simultaneously infiltrated with
438 Agrobacteria carrying the relevant constructs *35Spro::*RGH2-FLAG, *35Spro::*RGH2^{+}-
439 FLAG, *35Spro::*RGH3-HA and *MASpro::*GFP-AVR-Pii from wheat and rice or
440 *35Spro::*GFP-HA and *MASpro::*GFP-AVR-Pii^{F65E} as controls. The Agrobacterium
441 strains were resuspended in ARM buffer (Agrobacterium resuspension medium)
442 containing 10 mM MES (pH 5.6), 10 mM MgCl2, and 150 μM acetosyringone. The
443 optical density at 600 nm (OD_{600}) was adjusted as follows: RGH2/RGH2^{+} and RGH3
444 at 0.4, effectors and controls at 0.6, and p19 at 0.1. Two leaves from each *N.*
445 *benthamiana* plant were infiltrated using a needleless syringe. Leaves were harvested
446 at 3 days post-infiltration (dpi), and UV fluorescence images were captured from the
447 abaxial side. Imaging was conducted using a Nikon D4 camera equipped with a 60-
448 mm macro lens, with ISO set at 1600 and an exposure time of approximately 10
449 seconds at F14. A Kodak Wratten No.8 filter was used, and the white balance was set
450 to 6,250 °K. Illumination was provided by Blak–Ray longwave (365 nm) B-100AP
451 spotlight lamps, which were moved around the subject during exposure to ensure even
452 illumination. The presented images are representative of three independent
453 experiments, each with a minimum of 6 leaves analysed.

454 **Ion leakage assays**

455 Leaves of *N. benthamiana* were infiltrated with either *35Spro::*RGH2-FLAG or
456 *35Spro::*RGH2^{+}-FLAG in combination with *MASpro::*RGH3-HA and either
457 *MASpro::*GFP-AVR-Pii or *MASpro::*GFP-AVR-Pii$^{Phe/Glu}$ from both rice and wheat blast.
458 Ion leakage assays were performed as described in Hatsugai and Katagiri (2018)[67].
459 Briefly, measurements were performed after 4, 24 and 48 hours post-harvest with a

460 compact conductivity meter (LAQUAtwin-EC-33, Horiba Scientific). Five leaf discs
461 (4mm diameter) were harvested from different leaves and immersed inside 2ml ddH_2O
462 as one biological replicate. Each measurement contains five biological replicates, and
463 all experiments were performed at least three times.

464 **Split GAL4 RUBY assay**

465 To detect protein-protein binding in *N. benthamiana* we performed the split GAL4
466 RUBY assay according to Chen *et al*., 2023.[51] Briefly, Agrobacterium containing
467 OsExo70F3, RGH2-Exo70 and $RGH2^+$-Exo70 (residues 1033-1637) fused to the
468 yeast GAL4 DNA binding domain protein under the *35S* promoter. Wheat and rice blast
469 AVR-Pii and the mutants or ZiF_IIb were fused to the herpes virus VP16 AD either
470 under the *35S* promoter or *MAS* promoter. *N. benthamiana* leaves were harvested
471 after 3dpi. To extract betalain, harvested plant leaves were completely immersed in
472 100% ethanol until all chlorophyll was removed. A diameter of 0.8 cm was taken from
473 each infiltration site and put into H_20. Extracted betalain accumulation was measured
474 in a Greiner F-bottom clear plate in a microplate reader (Clariostar, BMG Labtech) at
475 538 nm wavelength. All experiments were performed with five plants and repeated at
476 least 3 times.

477 To confirm protein expression, plant samples were harvested 3 dpi, ground in liquid
478 nitrogen and heated for 10 min at 70 °C in LDS buffer (Bio-Rad Laboratories, USA).
479 Samples were centrifugated and the supernatant was subjected to SDS-PAGE gels
480 and western blot. The membranes were probed with anti-GAL4 DNA-BD_HRP (Santa
481 Cruz Biotechnology) for OsExo70F3, RGH2-Exo70 and $RGH2^+$-Exo70 and with the
482 anti-VP16 antibody (Sigma-Aldrich, USA, V4388) primary antibody and Goat anti-
483 rabbit as secondary antibody (Sigma-Aldrich, USA, 12-348) for the effectors.

484 **Co-immunoprecipitation**

485 Transient gene expression in planta was performed by co-infiltrating 4-week-old *N.*
486 *benthamiana* plants with *A. tumefaciens* strain GV3101 carrying *35Spro::*OsExo70F3-
487 FLAG or *35Spro::*RGH2-Exo70-FLAG with rice AVR-Pii, the wheat blast variant or their
488 respective mutants. NLRs *MASpro::*FLAG-RGH2, *MASpro::*FLAG-$RGH2^+$,
489 *MASpro::*HA-RGH3 and rice AVR-Pii, the wheat blast variant, or their respective
490 mutants, and ZiF_IIb under the *MAS* promoter (Fig. 3D and Fig. S9) were infiltrated at
491 OD_{600} 0.4 and 0.6, respectively, in ARM buffer (Agrobacterium resuspension medium,

492 10 mM MgCl2, 10 mM 2-(N-morpholine)-ethanesulfonic acid [MES], and pH 5.6) with
493 the addition of 150 μM acetosyringone. Two leaves from each *N. benthamiana* plant
494 were infiltrated and 48 h later, samples were harvested and frozen in liquid nitrogen.
495 Total proteins were extracted from 450 mg tissue samples and suspended in 2 mL
496 GTEN buffer (25 mM Tris pH 7.5, 150 mM NaCl, 1 mM EDTA, 10% v/v glycerol, 2%
497 w/v PVPP, 10 mM DTT, 1 × complete protease inhibitor tablet per 50 mL (Roche), and
498 0.1% Tween 20). Extracts were cleared by centrifugation at 4000 xg at 4 °C for 30 min.
499 Protein pull downs were performed by adding 30 μL of anti-FLAG magnetic beads
500 using M2 anti-FLAG magnetic beads (Sigma). Briefly, samples were incubated in a
501 rotary mixer for 1h at 4 °C, washed afterwards 5 times with 1 ml IP buffer (25 mM Tris
502 pH 7.5, 150 mM NaCl, 1 mM EDTA, 10% glycerol, and 0.1% Tween 20) and proteins
503 were eluted by incubating the beads at 70°C in 30 μL of LDS RunBlue sample buffer
504 for 10 mins. About 15–20 μL of the extracts were analysed by SDS-PAGE followed by
505 immunoblot using either anti-FLAG (Cohesion Biosciences, at 1:3000 dilution), anti-
506 GFP (Santa Cruz Biotechnology, at 1:3000 dilution) or HA-probe (Santa Cruz
507 Biotechnology, 1:5000 dilution). Experiments were repeated at least three times.

508 **Protein immunoblotting**

509 Protein samples were prepared from five tissue discs (8 mm diameter) sampled from
510 *N. benthamiana* leaves at 2 or 3 days after agroinfiltration and were homogenized in
511 100 μL of 2X LDS loading buffer (Bio-Rad). Proteins were transferred onto a PVDF
512 (polyvinylidene difluoride) membrane using Trans-Blot Turbo transfer system (Bio-
513 Rad) according to the manufacturer's protocol. Immunoblotting was performed with
514 HA-probe (Santa Cruz Biotechnology, 1:5000 dilution), anti-GFP antibody ((Santa
515 Cruz Biotechnology, at 1:3000 dilution) or anti-FLAG (Cohesion Biosciences, at 1:3000
516 dilution). Proteins were visualized using Clarity Max Western ECL Substrate (Bio Rad)
517 in the ImageQuant LAS 500 spectrophotometer (GE Healthcare). Total protein loading
518 was visualized by staining the PVDF membrane with Ponceau S solution (Sigma-
519 Aldrich, P7170).

520 **Yeast two-hybrid assay**

521 To examine the interaction between all Exo70s and effectors we used the Matchmaker
522 Gold system (Takara Bio, USA) following the manufacturer's protocol. The proteins
523 were cloned into pGBKT7 or pGADT7 vectors, respectively. Exo70 integrated domains

524 RGH2-Exo70 (residues 1033-1637), RGH2^{+}-Exo70 (residues 1033-1637), Apu28443-
525 Exo70 (residues 990-1644), Hla80948-Exo70 (residues 765-1269), Hvu23924-Exo70
526 (residues 726-1321), Jef9120-Exo70 (residues 364-887) were cloned into pGBKT7 for
527 GAL4 binding domain fusion. OsExo70F3 in pGBKT7 and ZiF effectors and mutants
528 in pGADT7 were previously generated[32]. Constructs were co-transformed into
529 chemically competent Y2HGold cells using a Frozen-EZ Yeast transformation II Kit
530 (Zymo research, USA). We selected yeast co-transformants on selective dropout (SD)
531 media lacking only Trp and Leu. Protein interactions were assessed on SD selection
532 medium lacking Trp, Leu, His and Ade containing X-α-Gal and supplemented with 0.2
533 ug/ml Aureobasidin A (Takara Bio, USA). Plates were incubated on 30 °C and
534 interaction was observed 4 days later. Each experiment was repeated a minimum of
535 three times with similar results.

536 To confirm protein expression, total yeast extracts from transformed colonies were
537 produced by heating the cells for 10 min at 70 °C in LDS buffer (Bio-Rad Laboratories,
538 USA). Samples were centrifugated and the supernatant was subjected to SDS-PAGE
539 gels and western blot. The membranes were probed with anti-GAL4 DNA-BD (Sigma
540 Aldrich, USA, G3042) for OsExo70F3, RGH2-Exo70, RGH2^{+}-Exo70, Apu28443-
541 Exo70, Hla80948-Exo70, Hvu23924-Exo70, Jef9120-Exo70 proteins in pGBKT7 and
542 with the anti-GAL4 activation domain (Sigma Aldrich, USA, G9293) antibodies for
543 effectors in pGADT7.

544 **Protein expression and purification**

545 RGH2-Exo70 and RGH2^{+}-Exo70 domains (residues 1033-1637) were 6xHis-SUMO-
546 tagged and produced in *E. coli* Rosetta™ (DE3) and AVR-Pii variants were 6xHis-
547 MBP-tagged and produced in *E. coli* SHuffle cells using established protocols[29]. All
548 tags were added at the N-terminus. In brief, cell cultures were grown in LB media at
549 37 °C for Rosetta and 30 °C for SHuffle cells for 5–7 hr and then at 16 °C overnight.
550 Cells were harvested by centrifugation (10 min, 5500x g, 4 °C) and re-suspended in
551 50 mM Tris-HCl (pH 7.5), 500 mM NaCl, 50 mM glycine, 5% (vol/vol) glycerol, and 20
552 mM imidazole supplemented with cOmplete EDTA-free Protease Inhibitor Cocktail
553 (Roche). Cells were lysed by sonication and clarified by centrifugation (50,000x g for
554 30 mins at 4 °C). Protein purification was carried out as previously described[29].

555 **Isothermal titration calorimetry**

556 ITC experiments were performed using a MicroCal PEAQ-ITC instrument (Malvern,
557 United Kingdom). For each experiment, 300 µL of RGH2-Exo70 or RGH2^{+}-Exo70
558 domains at a concentration of 20 µM was loaded into the calorimetric cell, while the
559 syringe contained 200 µM of either wheat or rice blast AVR-Pii or their Phe to Glu
560 mutants. Each run consisted of a single injection of 0.5 µL followed by 18 injections of
561 2 µL each, with intervals of 120 s between injections. The stirring speed was 750 rpm.
562 Data obtained from the experiments were analysed using AFFINImeter ITC software[68].
563 Both wild type and mutant samples were subjected to triplicate runs. The experiments
564 were conducted at 25 °C in a buffer containing 20 mM HEPES (pH 7.5), 150 mM NaCl,
565 and 5% (vol/vol) glycerol. The stability of RGH2/RGH2^{+} Exo70 domains on purification
566 likely affects the accurate measurement of stoichiometry on complex formation with
567 the effectors (1:1 expected based on the structure of OsExo70F2 with AVR-Pii).

568 ***M. oryzae* inoculation and plant phenotypic assays**

569 Protocols for culturing and inoculation of *M. oryzae* were similar to those previously
570 described[46,69,70]. Briefly, hyphal tips from culture plates were transferred to oatmeal
571 agar (20 g oatmeal, 10 g agar, 2.5 g sucrose, and addition of ddH2O to 500 mL) plates
572 (deep petri dish 100 × 20 mm) and incubated for 10 to 15 d at 24 °C to produce conidia.
573 Oatmeal plates were washed with 8 mL dH2O and conidia collected by gentle scraping
574 with the tip of a 1.5 mL tube. The suspension was filtered through Miracloth (Merck
575 Chemicals, Ref.: 475855-1r) and collected. Spore concentration was counted with a
576 hemocytometer and adjusted to 1 × 10^5 spores per milliliter in dH2O with 0.01% Tween
577 20 (Merck Chemicals, CAS Number: 9005-64-5).

578 For detached leaf assays, barley leaves were sampled and placed on agar in boxes
579 (2.5 g agar-agar [Fisher, CAS 9002-18-0]; 50 mL benzimidazole [1 g/1 L H2O stock
580 solution]; 450 mL H2OFor spray inoculations, the conidial suspension was sprayed
581 onto the leaves in each box using a small atomiser spray bottle with 3 - 4 sprays used
582 until droplets were observed on the leaf surface. Boxes were placed in a Sanyo cabinet
583 and maintained at 25 °C. Continuous light was used in the first 24 hrs and then, after
584 excess water was removed from droplets using sterile Miracloth, boxes were
585 maintained in a 16/8 hr light/dark cycle. Phenotypes were recorded at 7 dpi using a
586 macroscopic phenotype scale[46] (0 = complete resistance; 1 = small brown resistant

587 spots; 2 = susceptible larger eyespot lesions; 3 = larger spreading lesions; and 4 =
588 hypersusceptibility).

589 **Statistical analyses**

590 Graphs and statistical analysis (the Student's *t* test, Tukey's ANOVA, Two-Way
591 ANOVA) were performed using GraphPad Prism version 10.2.2 and R-Studio version
592 2024.04.2+764. Ordinal phenotyping data were analysed using a cumulative link
593 mixed model implemented in the R package ordinal (version 2023.12.4.1;
594 https://CRAN.R-project.org/package=ordinal)[71]. The model was specified as:
595 phenotype ~ accession + (1 | independent family) + (1 | replicate) + (1 |
596 replicate:independent family) where accession specifies Golden Promise control,
597 RGH2, or RGH2+ transgenic lines. The Laplace approximation was used for likelihood
598 estimation. Post hoc pairwise comparisons were conducted using the estimated
599 marginal means derived using the emmeans package (version 1.11.2.8;
600 https://CRAN.R-project.org/package=emmeans) and *p*-values were adjusted using
601 Tukey's method. Details of plots and statistical tests used are given in the appropriate
602 figure legends.

603 ## Data/Resource availability

604 Further information and requests for resources and reagents should be directed to the
605 Mark Banfield (mark.banfield@jic.ac.uk). There are no restrictions on the availability
606 of materials. Any additional information required to re-analyze the reported data is
607 available from the lead contact. The data, including FASTA, Phylip, and Nexus files
608 used for preparing Fig. 1 are available on Figshare
609 (www.doi.org/10.6084/m9.figshare.28057085). All other study data are included in the
610 article and/or Supplementary Information.

611 ## Acknowledgments

612 The authors thank the Biotechnology and Biological Sciences Research Council
613 (UKRI-BBSRC, UK, grants BB/V015508/1, BB/P012574, BBS/E/J/000PR9795,
614 BBS/E/J/000PR9796 and BB/X010996/1), the BBSRC Norwich Research Park
615 Biosciences Doctoral Training Partnership (grant BB/T008717/1), the John Innes
616 Foundation, the Gatsby Charitable Foundation, the United States Department of
617 Agriculture-Agricultural Research Service (CRIS #5062-21220-025-000D) and the

European Union Framework Programme for Research and Innovation Horizon 2020 (2014–2020) under the Marie Curie Skłodowska Grant Agreement Nr. 847548 for funding. The authors thank all members of the Banfield Laboratory for discussions, in particular Clemence Rodney for careful reading of the manuscript. The authors also thank Abbas Maqbool (JIC Biophysical Analysis), Carlo Martins and Gerhard Saalbach (JIC Proteomics), Julia Mundy (JIC Structural Biology), Phil Robinson (Scientific Photographer), Matt Smoker and Jodie Taylor (TSL Tissue Culture and Transformation), Mark Youles and Liam Egan (TSL SynBio) for their expert help and advice in this work.

Author Contributions:

I.S., H.J.B., M.J.M., J.C.D.C. and M.J.B. designed the experiments; I.S., H.J.B., J.W.B., A.H.C.L., I.H, M.J.M. and J.C.D.C. performed the experiments; I.S., H.J.B., J.W.B., A.H.C.L., I.H., M.J.M., J.C.D.C. and M.J.B. wrote and reviewed the manuscript.

Declaration of Interests

The authors declare no competing interests.

References

(1) Wilson, R. A.; Talbot, N. J. Under Pressure: Investigating the Biology of Plant Infection by Magnaporthe Oryzae. *Nat. Rev. Microbiol.* **2009**, *7* (3), 185–195. https://doi.org/10.1038/nrmicro2032.

(2) Latorre, S. M.; Were, V. M.; Foster, A. J.; Langner, T.; Malmgren, A.; Harant, A.; Asuke, S.; Reyes-Avila, S.; Gupta, D. R.; Jensen, C.; Ma, W.; Mahmud, N. U.; Mehebub, M. S.; Mulenga, R. M.; Muzahid, A. N. M.; Paul, S. K.; Rabby, S. M. F.; Rahat, A. A. M.; Ryder, L.; Shrestha, R.-K.; Sichilima, S.; Soanes, D. M.; Singh, P. K.; Bentley, A. R.; Saunders, D. G. O.; Tosa, Y.; Croll, D.; Lamour, K. H.; Islam, T.; Tembo, B.; Win, J.; Talbot, N. J.; Burbano, H. A.; Kamoun, S. Genomic Surveillance Uncovers a Pandemic Clonal Lineage of the Wheat Blast Fungus. *PLOS Biol.* **2023**, *21* (4), e3002052. https://doi.org/10.1371/journal.pbio.3002052.

(3) Maciel, J. L. N. Magnaporthe Oryzae, the Blast Pathogen: Current Status and Options for Its Control. *CABI Rev.* **2012**, *2011*, 1–8. https://doi.org/10.1079/PAVSNNR20116050.

(4) Igarashi, S. Pyricularia Em Trigo. 1. Ocorrencia de Pyricularia Sp Noestado Do Parana. *Fitopatol.Bras* **1986**, *11*, 351–352.

(5) Singh, P. K.; Gahtyari, N. C.; Roy, C.; Roy, K. K.; He, X.; Tembo, B.; Xu, K.; Juliana, P.; Sonder, K.; Kabir, M. R.; Chawade, A. Wheat Blast: A Disease Spreading by Intercontinental Jumps and Its Management Strategies. *Front. Plant Sci.* **2021**, *12*. https://doi.org/10.3389/fpls.2021.710707.

(6) Bentham, A. R.; De la Concepcion, J. C.; Benjumea, J. V.; Kourelis, J.; Jones, S.; Mendel, M.; Stubbs, J.; Stevenson, C. E. M.; Maidment, J. H. R.; Youles, M.; Zdrzałek, R.; Kamoun, S.; Banfield, M. J. Allelic Compatibility in Plant Immune Receptors Facilitates Engineering of New Effector Recognition Specificities. *Plant Cell* **2023**, *35* (10), 3809–3827. https://doi.org/10.1093/plcell/koad204.

(7) Kourelis, J.; Marchal, C.; Posbeyikian, A.; Harant, A.; Kamoun, S. NLR Immune Receptor–Nanobody Fusions Confer Plant Disease Resistance. *Science* **2023**, *379* (6635), 934–939. https://doi.org/10.1126/science.abn4116.

(8) Zdrzałek, R.; Stone, C.; De la Concepcion, J. C.; Banfield, M. J.; Bentham, A. R. Pathways to Engineering Plant Intracellular NLR Immune Receptors. *Curr. Opin. Plant Biol.* **2023**, *74*, 102380. https://doi.org/10.1016/j.pbi.2023.102380.

(9) Cadiou, L.; Brunisholz, F.; Cesari, S.; Kroj, T. Molecular Engineering of Plant Immune Receptors for Tailored Crop Disease Resistance. *Curr. Opin. Plant Biol.* **2023**, *74*, 102381. https://doi.org/10.1016/j.pbi.2023.102381.

(10) Jones, J. D. G.; Vance, R. E.; Dangl, J. L. Intracellular Innate Immune Surveillance Devices in Plants and Animals. *Science* **2016**, *354* (6316), aaf6395. https://doi.org/10.1126/science.aaf6395.

(11) Jubic, L. M.; Saile, S.; Furzer, O. J.; El Kasmi, F.; Dangl, J. L. Help Wanted: Helper NLRs and Plant Immune Responses. *Curr. Opin. Plant Biol.* **2019**, *50*, 82–94. https://doi.org/10.1016/j.pbi.2019.03.013.

(12) Adachi, H.; Derevnina, L.; Kamoun, S. NLR Singletons, Pairs, and Networks: Evolution, Assembly, and Regulation of the Intracellular Immunoreceptor Circuitry of Plants. *Curr. Opin. Plant Biol.* **2019**, *50*, 121–131. https://doi.org/10.1016/j.pbi.2019.04.007.

(13) Ashikawa, I.; Hayashi, N.; Yamane, H.; Kanamori, H.; Wu, J.; Matsumoto, T.; Ono, K.; Yano, M. Two Adjacent Nucleotide-Binding Site–Leucine-Rich Repeat Class Genes Are Required to Confer Pikm-Specific Rice Blast Resistance. *Genetics* **2008**, *180* (4), 2267–2276. https://doi.org/10.1534/genetics.108.095034.

(14) Maqbool, A.; Saitoh, H.; Franceschetti, M.; Stevenson, C.; Uemura, A.; Kanzaki, H.; Kamoun, S.; Terauchi, R.; Banfield, M. Structural Basis of Pathogen Recognition by an Integrated HMA Domain in a Plant NLR Immune Receptor. *eLife* **2015**, *4*, e08709. https://doi.org/10.7554/eLife.08709.

(15) Césari, S.; Thilliez, G.; Ribot, C.; Chalvon, V.; Michel, C.; Jauneau, A.; Rivas, S.; Alaux, L.; Kanzaki, H.; Okuyama, Y.; Morel, J.-B.; Fournier, E.; Tharreau, D.; Terauchi, R.; Kroj, T. The Rice Resistance Protein Pair RGA4/RGA5 Recognizes the Magnaporthe Oryzae Effectors AVR-Pia and AVR1-CO39 by Direct Binding. *Plant Cell* **2013**, *25* (4), 1463–1481. https://doi.org/10.1105/tpc.112.107201.

(16) Césari, S.; Kanzaki, H.; Fujiwara, T.; Bernoux, M.; Chalvon, V.; Kawano, Y.; Shimamoto, K.; Dodds, P.; Terauchi, R.; Kroj, T. The NB-LRR Proteins RGA4 and RGA5 Interact Functionally and Physically to Confer Disease Resistance. *EMBO J.* **2014**, *33* (17), 1941–1959. https://doi.org/10.15252/embj.201487923.

(17) Zhang, X.; Liu, Y.; Yuan, G.; Wang, D.; Zhu, T.; Wu, X.; Ma, M.; Guo, L.; Guo, H.; Bhadauria, V.; Liu, J.; Peng, Y.-L. The Effector Recognition by Synthetic Sensor NLR Receptors Requires the Concerted Action of Multiple Interfaces within and Outside the Integrated Domain. bioRxiv August 18, 2022, p 2022.08.17.504349. https://doi.org/10.1101/2022.08.17.504349.

(18) De la Concepcion, J. C.; Franceschetti, M.; Maqbool, A.; Saitoh, H.; Terauchi, R.; Kamoun, S.; Banfield, M. J. Polymorphic Residues in Rice NLRs Expand Binding and Response to Effectors of the Blast Pathogen. *Nat. Plants* **2018**, *4* (8), 576–585. https://doi.org/10.1038/s41477-018-0194-x.

(19) De la Concepcion, J. C.; Franceschetti, M.; MacLean, D.; Terauchi, R.; Kamoun, S.; Banfield, M. J. Protein Engineering Expands the Effector Recognition Profile of a Rice NLR Immune Receptor. *eLife* **2019**, *8*, e47713. https://doi.org/10.7554/eLife.47713.

(20) Maidment, J. H.; Shimizu, M.; Bentham, A. R.; Vera, S.; Franceschetti, M.; Longya, A.; Stevenson, C. E.; De la Concepcion, J. C.; Białas, A.; Kamoun, S.; Terauchi, R.; Banfield, M. J. Effector Target-Guided Engineering of an Integrated Domain Expands the Disease Resistance Profile of a Rice NLR Immune Receptor. *eLife* **2023**, *12*, e81123. https://doi.org/10.7554/eLife.81123.

(21) Kanzaki, H.; Yoshida, K.; Saitoh, H.; Fujisaki, K.; Hirabuchi, A.; Alaux, L.; Fournier, E.; Tharreau, D.; Terauchi, R. Arms Race Co-Evolution of Magnaporthe Oryzae AVR-Pik and Rice Pik Genes Driven by Their Physical Interactions. *Plant J.* **2012**, *72* (6), 894–907. https://doi.org/10.1111/j.1365-313X.2012.05110.x.

(22) De la Concepcion, J. C.; Vega Benjumea, J.; Bialas, A.; Terauchi, R.; Kamoun, S.; Banfield, M. J. Functional Diversification Gave Rise to Allelic Specialization in a Rice NLR Immune Receptor Pair. *eLife* **2021**, *10*, e71662. https://doi.org/10.7554/eLife.71662.

(23) Maidment, J. H. R.; Franceschetti, M.; Maqbool, A.; Saitoh, H.; Jantasuriyarat, C.; Kamoun, S.; Terauchi, R.; Banfield, M. J. Multiple Variants of the Fungal Effector AVR-Pik Bind the HMA Domain of the Rice Protein OsHIPP19, Providing a Foundation to Engineer Plant Defense. *J. Biol. Chem.* **2021**, *296*. https://doi.org/10.1016/j.jbc.2021.100371.

(24) Zdrzałek, R.; Xi, Y.; Langner, T.; Bentham, A. R.; Petit-Houdenot, Y.; De la Concepcion, J. C.; Harant, A.; Shimizu, M.; Were, V.; Talbot, N. J.; Terauchi, R.; Kamoun, S.; Banfield, M. J. Bioengineering a Plant NLR Immune Receptor with a Robust Binding Interface toward a Conserved Fungal Pathogen Effector. *Proc. Natl. Acad. Sci.* **2024**, *121* (28), e2402872121. https://doi.org/10.1073/pnas.2402872121.

(25) Guo, L.; Cesari, S.; de Guillen, K.; Chalvon, V.; Mammri, L.; Ma, M.; Meusnier, I.; Bonnot, F.; Padilla, A.; Peng, Y.-L.; Liu, J.; Kroj, T. Specific Recognition of Two MAX Effectors by Integrated HMA Domains in Plant Immune Receptors Involves Distinct Binding Surfaces. *Proc. Natl. Acad. Sci.* **2018**, *115* (45), 11637–11642. https://doi.org/10.1073/pnas.1810705115.

(26) Okuyama, Y.; Kanzaki, H.; Abe, A.; Yoshida, K.; Tamiru, M.; Saitoh, H.; Fujibe, T.; Matsumura, H.; Shenton, M.; Galam, D. C.; Undan, J.; Ito, A.; Sone, T.; Terauchi, R. A Multifaceted Genomics Approach Allows the Isolation of the Rice Pia-Blast Resistance Gene Consisting of Two Adjacent NBS-LRR Protein Genes. *Plant J.* **2011**, *66* (3), 467–479. https://doi.org/10.1111/j.1365-313X.2011.04502.x.

(27) Ortiz, D.; de Guillen, K.; Cesari, S.; Chalvon, V.; Gracy, J.; Padilla, A.; Kroj, T. Recognition of the Magnaporthe Oryzae Effector AVR-Pia by the Decoy Domain of the Rice NLR Immune Receptor RGA5. *Plant Cell* **2017**, *29* (1), 156–168. https://doi.org/10.1105/tpc.16.00435.

(28) Liu, Y.; Zhang, X.; Yuan, G.; Wang, D.; Zheng, Y.; Ma, M.; Guo, L.; Bhadauria, V.; Peng, Y.-L.; Liu, J. A Designer Rice NLR Immune Receptor Confers Resistance to the Rice Blast Fungus Carrying Noncorresponding Avirulence Effectors. *Proc. Natl. Acad. Sci.* **2021**, *118* (44), e2110751118. https://doi.org/10.1073/pnas.2110751118.

(29) De la Concepcion, J. C.; Fujisaki, K.; Bentham, A. R.; Cruz Mireles, N.; Sanchez de Medina Hernandez, V.; Shimizu, M.; Lawson, D. M.; Kamoun, S.; Terauchi, R.; Banfield, M. J. A Blast Fungus Zinc-Finger Fold Effector Binds to a Hydrophobic Pocket in Host Exo70 Proteins to Modulate Immune Recognition in Rice. *Proc. Natl. Acad. Sci.* **2022**, *119* (43), e2210559119. https://doi.org/10.1073/pnas.2210559119.

(30) Fujisaki, K.; Abe, Y.; Ito, A.; Saitoh, H.; Yoshida, K.; Kanzaki, H.; Kanzaki, E.; Utsushi, H.; Yamashita, T.; Kamoun, S.; Terauchi, R. Rice Exo70 Interacts with a Fungal Effector, AVR-Pii, and Is Required for AVR-Pii-Triggered Immunity. *Plant J.* **2015**, *83* (5), 875–887. https://doi.org/10.1111/tpj.12934.

(31) Fujisaki, K.; Abe, Y.; Sugihara, Y.; Nemoto, K.; Ito, K.; Kanzaki, E.; Ishikawa, K.; Iwai, M.; Utsushi, H.; Saitoh, H.; Takagi, H.; Takeda, T.; Abe, A.; Zheng, S.; Bialas, A.; Banfield, M. J.; Kamoun, S.; Terauchi, R. Binding of a Pathogen Effector to Rice Exo70 Proteins Tethered to the NOI/RIN4 Integrated Domain of the NLR Receptor Pii2 Confers Immunity against Fungi. bioRxiv August 27, 2024, p 239400. https://doi.org/10.1101/239400.

(32) De la Concepcion, J. C.; Langner, T.; Fujisaki, K.; Yan, X.; Were, V.; Lam, A. H. C.; Saado, I.; Brabham, H. J.; Win, J.; Yoshida, K.; Talbot, N. J.; Terauchi, R.; Kamoun, S.; Banfield, M. J. Zinc-Finger (ZiF) Fold Secreted Effectors Form a Functionally Diverse Family across Lineages of the Blast Fungus Magnaporthe Oryzae. *PLOS Pathog.* **2024**, *20* (6), e1012277. https://doi.org/10.1371/journal.ppat.1012277.

(33) Saeed, B.; Brillada, C.; Trujillo, M. Dissecting the Plant Exocyst. *Curr. Opin. Plant Biol.* **2019**, *52*, 69–76. https://doi.org/10.1016/j.pbi.2019.08.004.

(34) Mei, K.; Guo, W. The Exocyst Complex. *Curr. Biol.* **2018**, *28* (17), R922–R925. https://doi.org/10.1016/j.cub.2018.06.042.

(35) Cvrčková, F.; Grunt, M.; Bezvoda, R.; Hála, M.; Kulich, I.; Rawat, A.; Zárský, V. Evolution of the Land Plant Exocyst Complexes. *Front. Plant Sci.* **2012**, *3*, 159. https://doi.org/10.3389/fpls.2012.00159.

(36) Žárský, V.; Sekereš, J.; Kubátová, Z.; Pečenková, T.; Cvrčková, F. Three Subfamilies of Exocyst EXO70 Family Subunits in Land Plants: Early Divergence and Ongoing Functional Specialization. *J. Exp. Bot.* **2020**, *71* (1), 49–62. https://doi.org/10.1093/jxb/erz423.

(37) Žárský, V.; Kulich, I.; Fendrych, M.; Pečenková, T. Exocyst Complexes Multiple Functions in Plant Cells Secretory Pathways. *Curr. Opin. Plant Biol.* **2013**, *16* (6), 726–733. https://doi.org/10.1016/j.pbi.2013.10.013.

(38) De la Concepcion, J. C.; Duverge, H.; Kim, Y.; Julian, J.; Xu, H. D.; Ikene, S. A.; Bianchi, A.; Grujic, N.; Papareddy, R. K.; Grishkovskaya, I.; Haselbach, D.; Murray, D. H.; Clavel, M.; Irwin, N. A. T.; Dagdas, Y. Electrostatic Changes Enabled the Diversification of an Exocyst Subunit via Protein Complex Escape. bioRxiv August 26, 2024, p 2024.08.26.609756. https://doi.org/10.1101/2024.08.26.609756.

(39) Stegmann, M.; Anderson, R. G.; Westphal, L.; Rosahl, S.; McDowell, J. M.; Trujillo, M. The Exocyst Subunit Exo70B1 Is Involved in the Immune Response of Arabidopsis Thaliana to Different Pathogens and Cell Death. *Plant Signal. Behav.* **2013**, *8* (12), e27421. https://doi.org/10.4161/psb.27421.

(40) Pecenková, T.; Hála, M.; Kulich, I.; Kocourková, D.; Drdová, E.; Fendrych, M.; Toupalová, H.; Zársky, V. The Role for the Exocyst Complex Subunits Exo70B2 and Exo70H1 in the Plant-Pathogen Interaction. *J. Exp. Bot.* **2011**, *62* (6), 2107–2116. https://doi.org/10.1093/jxb/erq402.

(41) Guo, J.; Xu, C.; Wu, D.; Zhao, Y.; Qiu, Y.; Wang, X.; Ouyang, Y.; Cai, B.; Liu, X.; Jing, S.; Shangguan, X.; Wang, H.; Ma, Y.; Hu, L.; Wu, Y.; Shi, S.; Wang, W.; Zhu, L.; Xu, X.; Chen, R.; Feng, Y.; Du, B.; He, G. Bph6 Encodes an Exocyst-Localized Protein and Confers Broad Resistance to Planthoppers in Rice. *Nat. Genet.* **2018**, *50* (2), 297–306. https://doi.org/10.1038/s41588-018-0039-6.

(42) Du, Y.; Overdijk, E. J. R.; Berg, J. A.; Govers, F.; Bouwmeester, K. Solanaceous Exocyst Subunits Are Involved in Immunity to Diverse Plant Pathogens. *J. Exp. Bot.* **2018**, *69* (3), 655–666. https://doi.org/10.1093/jxb/erx442.

(43) Holden, S.; Bergum, M.; Green, P.; Bettgenhaeuser, J.; Hernández-Pinzón, I.; Thind, A.; Clare, S.; Russell, J. M.; Hubbard, A.; Taylor, J.; Smoker, M.; Gardiner, M.; Civolani, L.; Cosenza, F.; Rosignoli, S.; Strugala, R.; Molnár, I.; Šimková, H.; Doležel, J.; Schaffrath, U.; Barrett, M.; Salvi, S.; Moscou, M. J. A Lineage-Specific Exo70 Is Required for Receptor Kinase–Mediated Immunity in Barley. *Sci. Adv.* **2022**, *8* (27), eabn7258. https://doi.org/10.1126/sciadv.abn7258.

(44) De la Concepcion, J. C. The Exocyst Complex Is an Evolutionary Battleground in Plant-Microbe Interactions. *Curr. Opin. Plant Biol.* **2023**, *76*, 102482. https://doi.org/10.1016/j.pbi.2023.102482.

(45) Césari, S.; Bernoux, M.; Moncuquet, P.; Kroj, T.; Dodds, P. N. A Novel Conserved Mechanism for Plant NLR Protein Pairs: The 'Integrated Decoy' Hypothesis. *Front. Plant Sci.* **2014**, *5*. https://doi.org/10.3389/fpls.2014.00606.

(46) Brabham, H. J.; Gómez De La Cruz, D.; Were, V.; Shimizu, M.; Saitoh, H.; Hernández-Pinzón, I.; Green, P.; Lorang, J.; Fujisaki, K.; Sato, K.; Molnár, I.; Šimková, H.; Doležel, J.; Russell, J.; Taylor, J.; Smoker, M.; Gupta, Y. K.; Wolpert, T.; Talbot, N. J.; Terauchi, R.; Moscou, M. J. Barley MLA3 Recognizes the Host-Specificity Effector Pwl2 from Magnaporthe Oryzae. *Plant Cell* **2024**, *36* (2), 447–470. https://doi.org/10.1093/plcell/koad266.

(47) Brabham, H. J.; Hernández-Pinzón, I.; Holden, S.; Lorang, J.; Moscou, M. J. An Ancient Integration in a Plant NLR Is Maintained as a Trans-Species Polymorphism. bioRxiv December 25, 2017, p 239541. https://doi.org/10.1101/239541.

(48) Kroj, T.; Chanclud, E.; Michel-Romiti, C.; Grand, X.; Morel, J.-B. Integration of Decoy Domains Derived from Protein Targets of Pathogen Effectors into Plant Immune Receptors Is Widespread. *New Phytol.* **2016**, *210* (2), 618–626. https://doi.org/10.1111/nph.13869.

(49) Sarris, P. F.; Cevik, V.; Dagdas, G.; Jones, J. D. G.; Krasileva, K. V. Comparative Analysis of Plant Immune Receptor Architectures Uncovers Host Proteins Likely Targeted by Pathogens. *BMC Biol.* **2016**, *14* (1), 8. https://doi.org/10.1186/s12915-016-0228-7.

(50) Abramson, J.; Adler, J.; Dunger, J.; Evans, R.; Green, T.; Pritzel, A.; Ronneberger, O.; Willmore, L.; Ballard, A. J.; Bambrick, J.; Bodenstein, S. W.; Evans, D. A.; Hung, C.-C.; O'Neill, M.; Reiman, D.; Tunyasuvunakool, K.; Wu, Z.; Žemgulytė, A.; Arvaniti, E.; Beattie, C.; Bertolli, O.; Bridgland, A.; Cherepanov, A.; Congreve, M.; Cowen-Rivers, A. I.; Cowie, A.; Figurnov, M.; Fuchs, F. B.; Gladman, H.; Jain, R.; Khan, Y. A.; Low, C. M. R.; Perlin, K.; Potapenko, A.; Savy, P.; Singh, S.; Stecula, A.; Thillaisundaram, A.; Tong, C.; Yakneen, S.; Zhong, E. D.; Zielinski, M.; Žídek, A.; Bapst, V.; Kohli, P.; Jaderberg, M.; Hassabis, D.; Jumper, J. M. Accurate Structure Prediction of Biomolecular Interactions with AlphaFold 3. *Nature* **2024**, *630* (8016), 493–500. https://doi.org/10.1038/s41586-024-07487-w.

(51) Chen, J.; Luo, M.; Hands, P.; Rolland, V.; Zhang, J.; Li, Z.; Outram, M.; Dodds, P.; Ayliffe, M. A Split GAL4 RUBY Assay for Visual in Planta Detection of Protein–Protein Interactions. *Plant J.* **2023**, *114* (6), 1209–1226. https://doi.org/10.1111/tpj.16234.

(52) Islam, M. T.; Gupta, D. R.; Hossain, A.; Roy, K. K.; He, X.; Kabir, M. R.; Singh, P. K.; Khan, Md. A. R.; Rahman, M.; Wang, G.-L. Wheat Blast: A New Threat to Food Security. *Phytopathol. Res.* **2020**, *2* (1), 28. https://doi.org/10.1186/s42483-020-00067-6.

(53) Brabham, H. J.; Hernández-Pinzón, I.; Yanagihara, C.; Ishikawa, N.; Komori, T.; Matny, O. N.; Hubbard, A.; Witek, K.; Feist, A.; Numazawa, H.; Green, P.; Dreiseitl, A.; Takemori, N.; Komari, T.; Freedman, R. P.; Steffenson, B.; van Esse, H. P.; Moscou, M. J. Discovery of Functional NLRs Using Expression Level, High-Throughput Transformation and Large-Scale Phenotyping. *Nat. Plants* **2025**, *11* (10), 2100–2114. https://doi.org/10.1038/s41477-025-02110-w.

(54) Callaway, E. Devastating Wheat Fungus Appears in Asia for First Time. *Nature* **2016**, *532* (7600), 421–422. https://doi.org/10.1038/532421a.

(55) Islam, M. T.; Croll, D.; Gladieux, P.; Soanes, D. M.; Persoons, A.; Bhattacharjee, P.; Hossain, Md. S.; Gupta, D. R.; Rahman, Md. M.; Mahboob, M. G.; Cook, N.; Salam, M. U.; Surovy, M. Z.; Sancho, V. B.; Maciel, J. L. N.; NhaniJúnior, A.; Castroagudín, V. L.; Reges, J. T. de A.; Ceresini, P. C.; Ravel, S.; Kellner, R.; Fournier, E.; Tharreau, D.; Lebrun, M.-H.; McDonald, B. A.; Stitt, T.; Swan, D.; Talbot, N. J.; Saunders, D. G. O.; Win, J.; Kamoun, S. Emergence of Wheat Blast in Bangladesh Was Caused by a South American Lineage of Magnaporthe Oryzae. *BMC Biol.* **2016**, *14* (1), 84. https://doi.org/10.1186/s12915-016-0309-7.

(56) Tembo, B.; Mulenga, R. M.; Sichilima, S.; M'siska, K. K.; Mwale, M.; Chikoti, P. C.; Singh, P. K.; He, X.; Pedley, K. F.; Peterson, G. L.; Singh, R. P.; Braun, H. J. Detection and Characterization of Fungus (Magnaporthe Oryzae Pathotype Triticum) Causing Wheat Blast Disease on Rain-Fed Grown Wheat (Triticum Aestivum L.) in Zambia. *PLOS ONE* **2020**, *15* (9), e0238724. https://doi.org/10.1371/journal.pone.0238724.

(57) Bohra, A.; Kilian, B.; Sivasankar, S.; Caccamo, M.; Mba, C.; McCouch, S. R.; Varshney, R. K. Reap the Crop Wild Relatives for Breeding Future Crops. *Trends Biotechnol.* **2022**, *40* (4), 412–431. https://doi.org/10.1016/j.tibtech.2021.08.009.

(58) Kim, S. H.; Qi, D.; Ashfield, T.; Helm, M.; Innes, R. W. Using Decoys to Expand the Recognition Specificity of a Plant Disease Resistance Protein. *Science* **2016**, *351* (6274), 684–687. https://doi.org/10.1126/science.aad3436.

(59) Le Roux, C.; Huet, G.; Jauneau, A.; Camborde, L.; Trémousaygue, D.; Kraut, A.; Zhou, B.; Levaillant, M.; Adachi, H.; Yoshioka, H.; Raffaele, S.; Berthomé, R.; Couté, Y.; Parker, J. E.; Deslandes, L. A Receptor Pair with an Integrated Decoy Converts Pathogen Disabling of Transcription Factors to Immunity. *Cell* **2015**, *161* (5), 1074–1088. https://doi.org/10.1016/j.cell.2015.04.025.

(60) Sarris, P. F.; Duxbury, Z.; Huh, S. U.; Ma, Y.; Segonzac, C.; Sklenar, J.; Derbyshire, P.; Cevik, V.; Rallapalli, G.; Saucet, S. B.; Wirthmueller, L.; Menke, F. L. H.; Sohn, K. H.; Jones, J. D. G. A Plant Immune Receptor Detects Pathogen Effectors That Target WRKY Transcription Factors. *Cell* **2015**, *161* (5), 1089–1100. https://doi.org/10.1016/j.cell.2015.04.024.

(61) Seong, K.; Krasileva, K. V. Prediction of Effector Protein Structures from Fungal Phytopathogens Enables Evolutionary Analyses. *Nat. Microbiol.* **2023**, *8* (1), 174–187. https://doi.org/10.1038/s41564-022-01287-6.

(62) Derbyshire, M. C.; Raffaele, S. Surface Frustration Re-Patterning Underlies the Structural Landscape and Evolvability of Fungal Orphan Candidate Effectors. *Nat. Commun.* **2023**, *14* (1), 5244. https://doi.org/10.1038/s41467-023-40949-9.

(63) Guillen, K. de; Ortiz-Vallejo, D.; Gracy, J.; Fournier, E.; Kroj, T.; Padilla, A. Structure Analysis Uncovers a Highly Diverse but Structurally Conserved Effector Family in Phytopathogenic Fungi. *PLOS Pathog.* **2015**, *11* (10), e1005228. https://doi.org/10.1371/journal.ppat.1005228.

(64) Seong, K.; Wei, W.; Sent, S. C.; Vega, B.; Dee, A.; Ramirez-Bernardino, G.; Kumar, R.; Parra, L.; Saur, I. M.; Krasileva, K. Resurrection of the Plant Immune Receptor Sr50 to Overcome Pathogen Immune Evasion. bioRxiv February 11, 2025, p 2024.08.07.607039. https://doi.org/10.1101/2024.08.07.607039.

(65) Cesari, S.; Xi, Y.; Declerck, N.; Chalvon, V.; Mammri, L.; Pugnière, M.; Henriquet, C.; de Guillen, K.; Chochois, V.; Padilla, A.; Kroj, T. New Recognition Specificity in a Plant Immune Receptor by Molecular Engineering of Its Integrated Domain. *Nat. Commun.* **2022**, *13* (1), 1524. https://doi.org/10.1038/s41467-022-29196-6.

(66) Lampropoulos, A.; Sutikovic, Z.; Wenzl, C.; Maegele, I.; Lohmann, J. U.; Forner, J. GreenGate - A Novel, Versatile, and Efficient Cloning System for Plant Transgenesis. *PLOS ONE* **2013**, *8* (12), e83043. https://doi.org/10.1371/journal.pone.0083043.

(67) Hatsugai, N.; Katagiri, F. Quantification of Plant Cell Death by Electrolyte Leakage Assay. *Bio-Protoc.* **2018**, *8* (5), e2758. https://doi.org/10.21769/BioProtoc.2758.

(68) Piñeiro, Á.; Muñoz, E.; Sabín, J.; Costas, M.; Bastos, M.; Velázquez-Campoy, A.; Garrido, P. F.; Dumas, P.; Ennifar, E.; García-Río, L.; Rial, J.; Pérez, D.; Fraga, P.; Rodríguez, A.; Cotelo, C. AFFINImeter: A Software to Analyze Molecular Recognition Processes from Experimental Data. *Anal. Biochem.* **2019**, *577*, 117–134. https://doi.org/10.1016/j.ab.2019.02.031.

(69) Parker, D.; Beckmann, M.; Enot, D. P.; Overy, D. P.; Rios, Z. C.; Gilbert, M.; Talbot, N.; Draper, J. Rice Blast Infection of Brachypodium Distachyon as a Model System to Study Dynamic Host/Pathogen Interactions. *Nat. Protoc.* **2008**, *3* (3), 435–445. https://doi.org/10.1038/nprot.2007.499.

(70) Jia, Y.; Valent, B.; Lee, F. N. Determination of Host Responses to Magnaporthe Grisea on Detached Rice Leaves Using a Spot Inoculation Method. *Plant Dis.* **2003**, *87* (2), 129–133. https://doi.org/10.1094/PDIS.2003.87.2.129.

(71) Christensen, R. H. B. Ordinal: Regression Models for Ordinal Data, 2024. https://cran.r-project.org/web/packages/ordinal/index.html (accessed 2025-10-30).

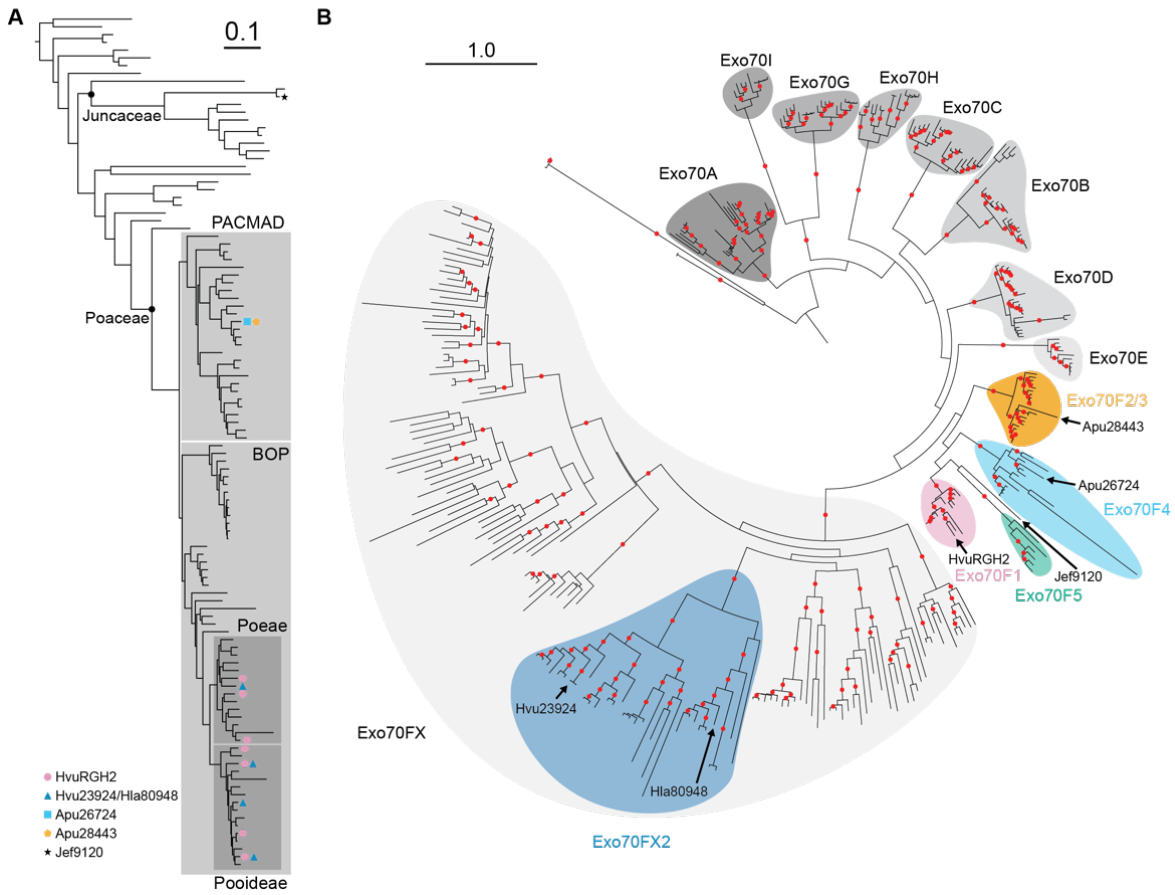

Fig. 1: NLRs with integrated Exo70 domains in the Poales are derived from the Exo70F and Exo70FX clades.

A. Maximum likelihood phylogenetic tree for Poales species based on 1,019 Benchmarking Universal Single-Copy Ortholog (BUSCO) genes from 110 species spanning 1,471,281 variable sites. Outgroup species include oilpalm (*Elaeis guineensis*) and banana (*Musa acuminata*). Legend indicates the presence of integrated Exo70 domains using coloured coded shapes. Important families, clades, and subfamilies in the Poales carrying integrated Exo70 domains are indicated in shaded boxes. Scale indicates substitutions per site.

B. Maximum likelihood phylogenetic tree of grass Exo70 proteins showing that integrated Exo70 domains are derived from the Exo70F and Exo70FX clades. Grass species include barley (*Hordeum vulgare*), wheat (*Triticum aestivum*), purple false brome (*Brachypodium distachyon*), rice (*Oryza sativa*), *Oropetium thomaeum*, maize (*Zea mays*), foxtail millet (*Setaria italica*), and sorghum (*Sorghum bicolor*). Exemplar integrated Exo70 domains include *H. vulgare* RGH2 (Exo70F1) and Hvu23934

930 (Exo70FX2), *Arundinella pubescens* Apu26724 (Exo70F4) and Apu28443 (Exo70F2),
931 *Holcus lanatus* Hla80948 (Exo70FX2), and *Juncus effusus* Jef9120 (unclassified
932 Exo70F). Outgroup Exo70s include *Saccharomyces cerevisiae* (yeast) and *Mus*
933 *musculus* (mouse). Scale indicates substitutions per site.

934

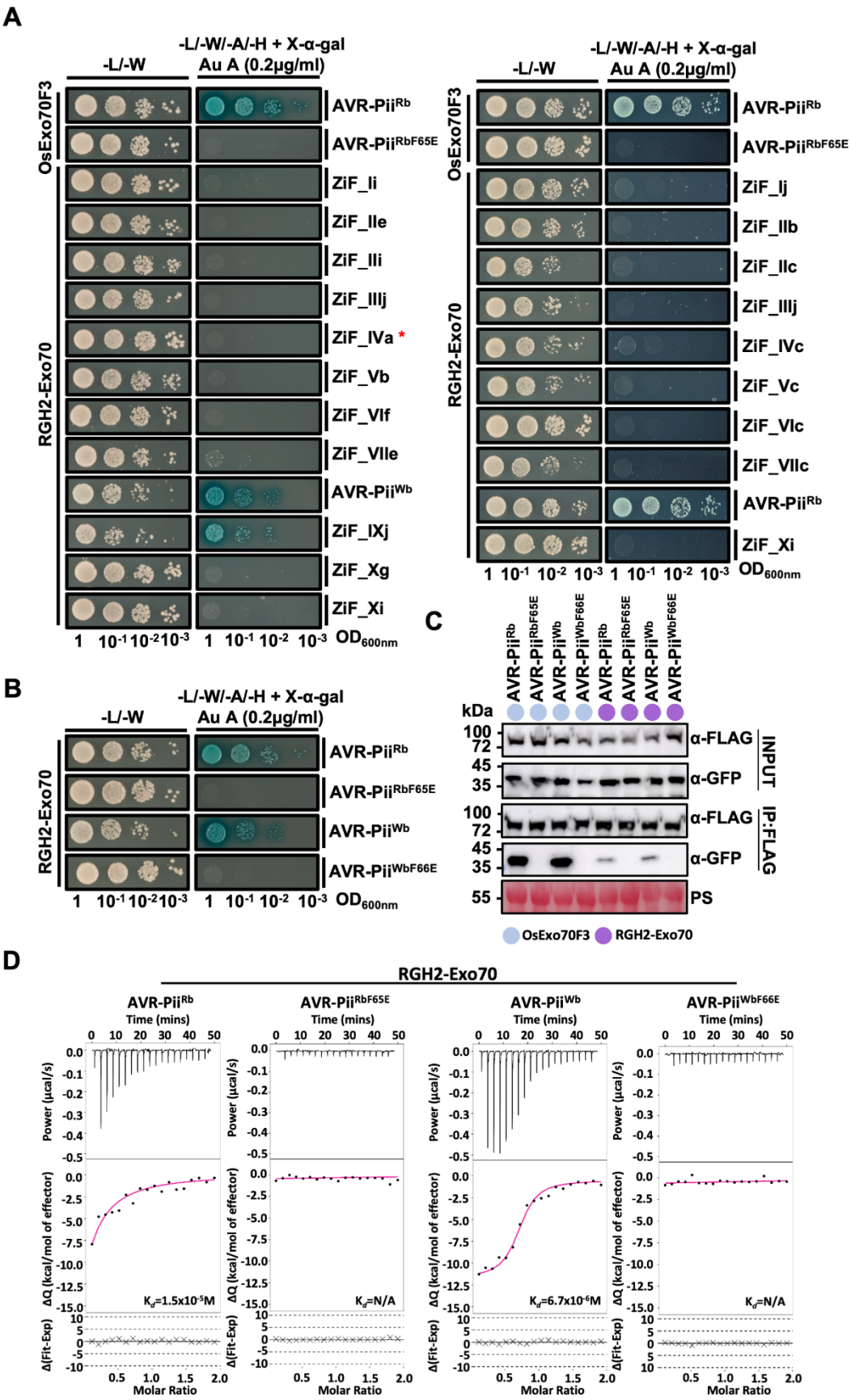

935

936 **Fig. 2: RGH2 interacts with rice blast AVR-Pii and the wheat blast variant in vitro**
937 **and in vivo.**

938 **A.** Y2H binding assay of the most prevalent ZiF effectors from wheat (left) and rice
939 (right) blast isolates as previously defined[32] to the RGH2-Exo70 integrated domain.
940 Yeast cells transformed with both plasmids were spotted onto selective synthetic
941 dropout (SD) media. For plates with quadruple-dropout media X-α-Gal and
942 Aureobasidin A (Au A) were added to the media. Yeast growth was monitored for
943 four days after plating. Growth and development of blue coloration indicates protein-
944 protein interactions. The experiment was repeated three times with comparable
945 results.

946 **B.** Interaction of rice blast AVR-Pii, the wheat blast variant and mutants with RGH2-
947 Exo70 using the Y2H assay. The experiment was carried out as described for panel
948 A. Yeast growth was monitored for four days subsequent to plating. The experiment
949 was repeated a minimum of three times, with similar results.

950 **C.** Co-IP assay showing that rice blast AVR-Pii and the wheat blast variant interact
951 with RGH2-Exo70-FLAG in *N. benthamiana.* The co-IP assays used an anti-FLAG
952 antibody to pull down AVR-Pii variants. Immunoblot analysis using an anti-GFP
953 antibody shows that RGH2-Exo70-FLAG and OsExo70F3-FLAG co-purified with rice
954 and wheat blast GFP-AVR-Pii variants but not with the effector mutants. Ponceau S
955 staining shows the total amount of protein loaded per lane in the input. The experiment
956 was repeated three times with similar results.

957 **D.** Binding of AVR-Pii variants to RGH2-Exo70 in vitro, as determined by ITC. Upper
958 panel shows the heat differences upon injection of AVR-Pii variants and mutants into
959 the cell containing RGH2-Exo70. Middle panel shows the integrated heats of injection
960 (dots-black colour) and best fit (solid line-magenta colour) to a single-site binding
961 model calculated using AFFINImeter ITC analysis software[68]. Bottom panel indicates
962 the difference between the fit to a single-site binding model and the experimental data.
963 The experiments shown are representative of three replicates.

964

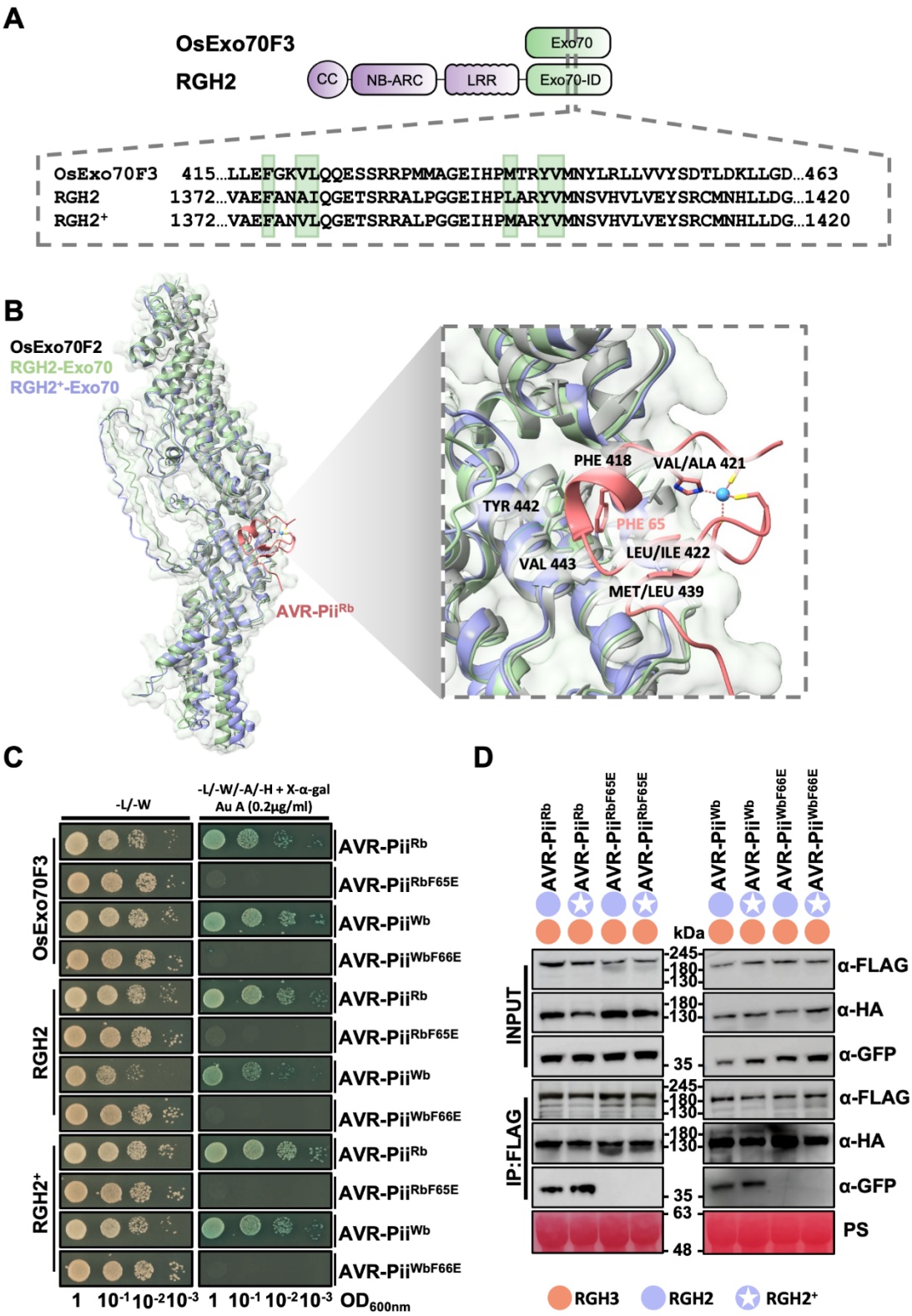

Fig. 3: RGH2⁺ binds rice blast AVR-Pii and the wheat blast variant.

A. Graphical representation of OsExo70F3 and the barley NLR RGH2. Sequence alignment of residues located at the effector binding interface in the OsExo70F2/AVR-Pii complex[29]. Residues important for the formation of the effector binding pocket are

971 highlighted in green. To generate the engineered NLR RGH2^{+}, amino acid mutations
972 Ala1378Val, Ile1379Leu, and Leu1396Met were made.

973 **B.** Left, Structural predictions generated with AlphaFold3 as used to interpret
974 interactions between AVR-Pii^{Rb} and RGH2-Exo70/RGH2^{+}-Exo70. The structure of
975 OsExo70F2 in complex with AVR-Pii^{Rb} (PDB:7pp2) was previously determined[29].
976 Right, zoom-in view of the binding interface in the OsExo70F2/AVR-Pii^{Rb} complex, with
977 RGH2-Exo70 and RGH2^{+}-Exo70 superimposed. The residues of OsExo70F2 involved
978 in binding the effector that are mutated in this study are indicated (Fig. 3A). The AVR-
979 Pii effector is shown in peach colour, with the Phe65 residue highlighted.

980 **C.** Y2H assay of rice blast AVR-Pii, the wheat blast variant, and mutants with
981 OsExo70F3, barley RGH2-Exo70 and RGH2^{+}-Exo70. Left, control plate for yeast
982 growth; right, the quadruple-dropout medium supplemented with X-α-Gal and
983 Aureobasidin A (Au A). The presence of yeast growth and the development of blue
984 coloration in the selection plate signify positive protein-protein interactions. Yeast
985 growth was monitored four days after plating. Each experiment was repeated at least
986 three times, with consistent results obtained.

987 **D.** Co-IP assay showing that rice blast AVR-Pii, and the wheat blast variant, interact
988 with full length RGH2 and RGH2^{+} co-expressed with the helper NLR RGH3 in *N.*
989 *benthamiana.* Co-IP assays were performed using an anti-FLAG antibody to pull down
990 RGH2-FLAG and RGH2^{+}-FLAG interacting proteins. Immunoblot analysis using an
991 anti-GFP antibody showed that GFP-AVR-Pii variants were pulled down with FLAG-
992 RGH2 and FLAG-RGH2^{+}, but mutant effectors showed no interaction. Anti-HA was
993 used to confirm the presence of RGH3-HA and interaction with RGH2. RGH2 and
994 RGH2^{+} were only detected weakly in the inputs, but immunoprecipitated proteins are
995 clear. Ponceau S staining shows the amount of total protein loaded per lane in the
996 input. An expanded blot with additional controls is shown in Supplementary Fig.9.
997 Experiment was repeated at least three times, with similar results obtained.

998

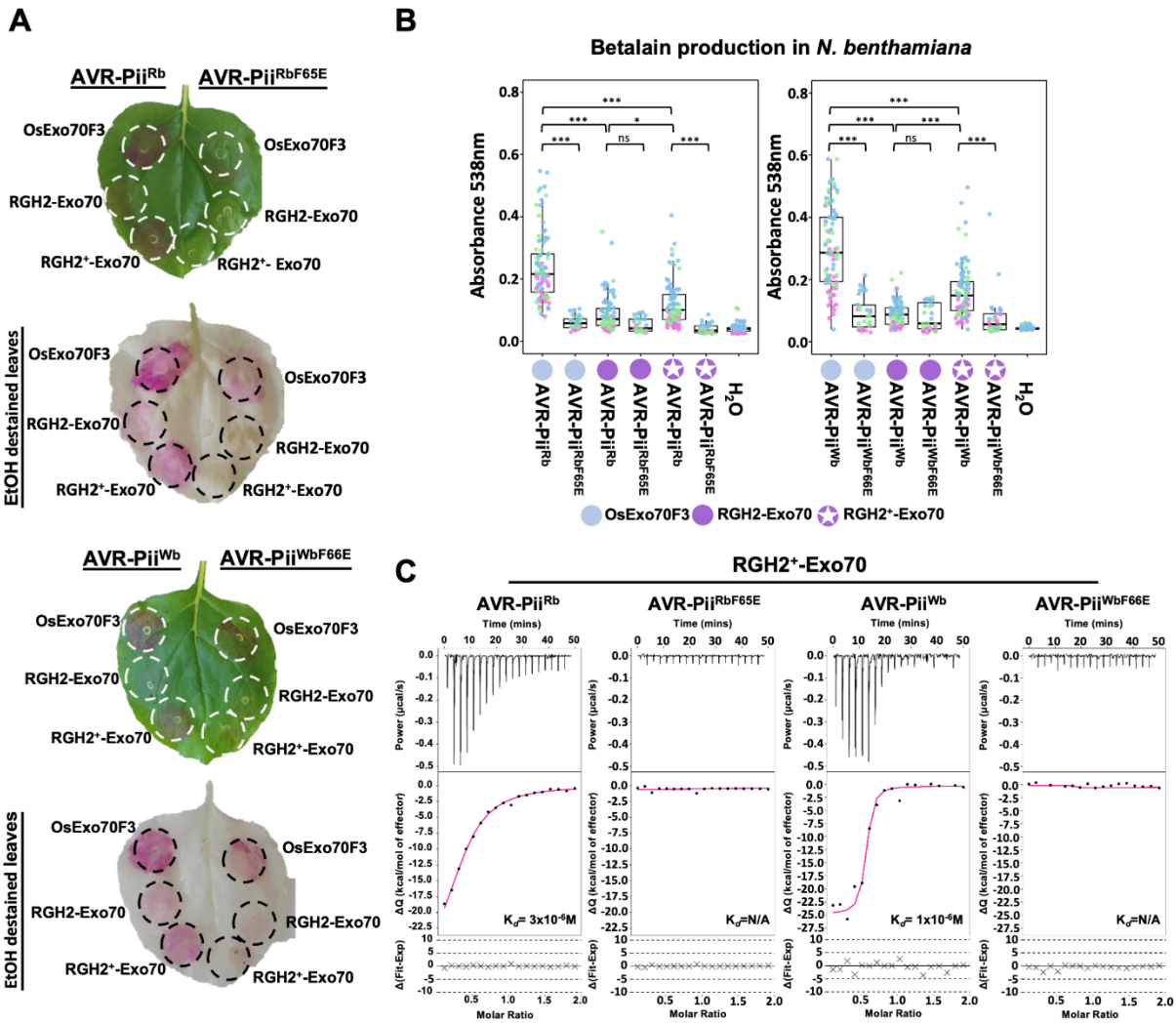

Fig. 4: AVR-Pii^{Wb} exhibits increased binding to RGH2^{+} compared with RGH2 in planta and in vitro.

A. Betalain production in *N. benthamiana* leaves following Agrobacterium infiltration with OsExo70F3-GAL4-BD, RGH2-Exo70-GAL4-BD or RGH2^{+}-Exo70-GAL4-BD and rice or wheat blast VP16-GAL4-AD-AVR-Pii variants or mutant effectors. Leaves expressing RGH2^{+} show increased betalain accumulation compared to RGH2 with AVR-Pii variants. Upper panels show brightfield images of *N. benthamiana* leaves three days post infiltration. Lower panel shows the same leaves cleared overnight in 100% ethanol. Infiltration points are marked with a white or black circle.

B. Leaves cleared with ethanol were used for betalain extraction. The absorbance for betalain production was measured at OD_{538nm} from independent infiltration sites for each construct combination. Replicates are designated with different colours (magenta-Replicate 1 (R1), green-Replicate 2 (R2), blue-Replicate 3 (R3)). Box plots

1014 represent the median (horizontal line), upper and lower quartiles (boxes), and 1.5×
1015 interquartile range (whiskers). Asterisks indicate statistically significant differences
1016 from the control (NS: not significant, *$p < 0.05$, **$p < 0.01$, ***$p < 0.001$, one-way
1017 ANOVA followed by Tukey's test). Data shown are from a pool of three biological
1018 replicates, n = 15 plants per pool (30 infiltration points per one biological replicate).

1019 **C.** Binding of rice blast AVR-Pii, the wheat blast variant, and mutants to RGH2^{+}-Exo70
1020 in vitro, as determined by ITC. Upper panel represents the heat differences upon
1021 injection of effector variants and mutants into the cell containing RGH2^{+}-Exo70. Middle
1022 panel shows the integrated heats of injection (dots - black colour) and best fit (solid
1023 line - magenta colour) to a single-site binding model calculated using AFFINImeter ITC
1024 analysis software[68]. Bottom panel indicates the difference between the fit to a single-
1025 site binding model and the experimental data. The experiments shown are
1026 representative of three replicates.

1027

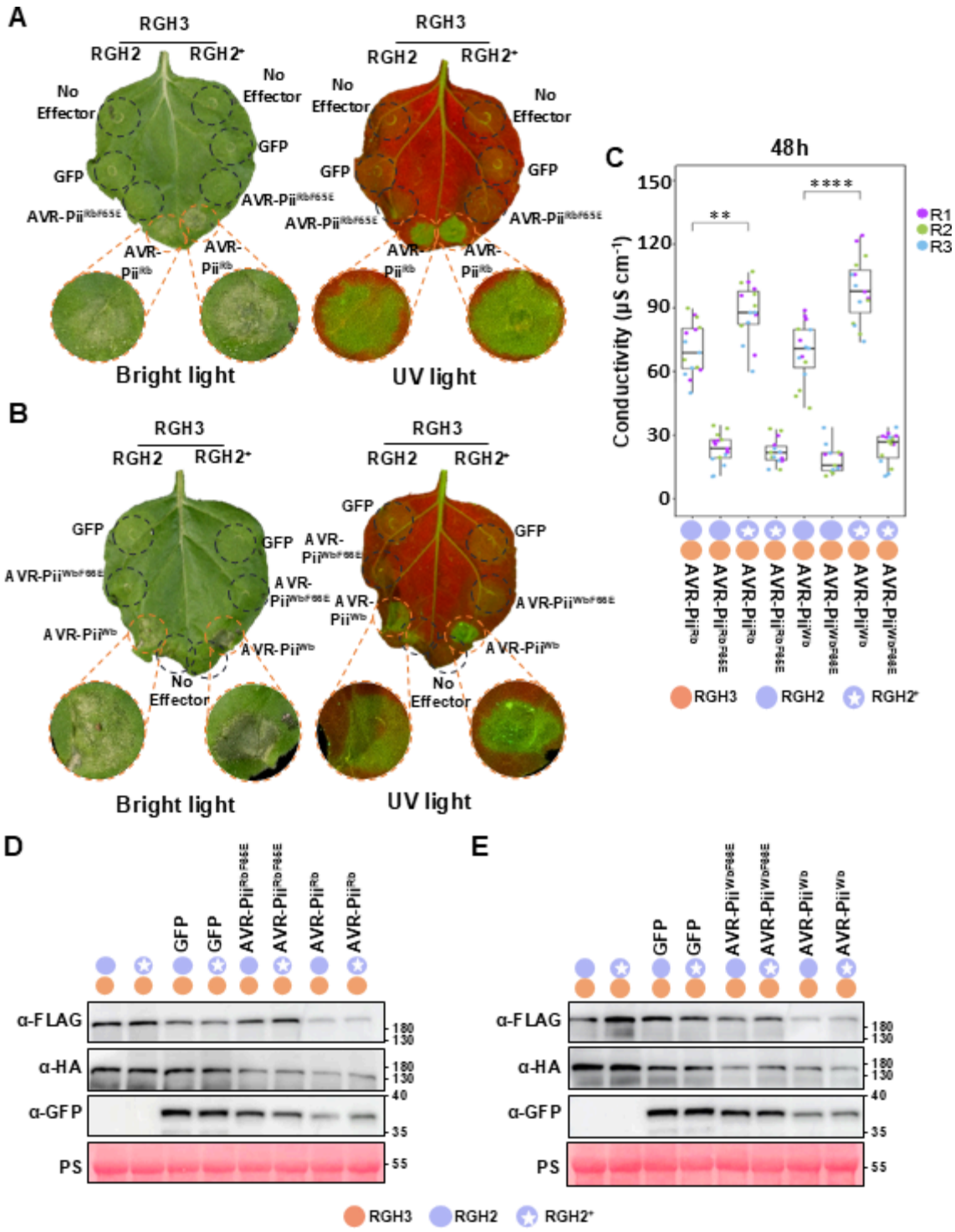

Fig. 5: RGH2⁺/RGH3 elicit an increased cell death response to rice blast AVR-Pii and the wheat blast variant compared to RGH2/RGH3.

A. Macroscopic cell death phenotypes observed on transient expression of RGH2/RGH3 or RGH2⁺/RGH3 NLR pairs with GFP, GFP-AVR-Pii^{Rb} or GFP-AVR-Pii^{RbF65E} mutant in *N. benthamiana*. Leaves were photographed five days post infiltration and are representative of three independent experiments.

1035 **B.** As for Fig. 5A but with the AVR-Pii^{Wb} variant and AVR-Pii^{WbF66E} mutant.

1036 **C.** Conductivity assay from *N. benthamiana* tissue infiltrated with RGH2/RGH3 or
1037 RGH2^{+}/RGH3 NLR pairs with rice or wheat blast GFP-AVR-Pii variants or mutants at
1038 48 hours post infiltration (hpi). Measurements of ion leakage after 4 and 24 hpi are
1039 shown in Supplementary Fig.12. Box plots represent the median (horizontal line),
1040 upper and lower quartiles (boxes), and 1.5× interquartile range (whiskers). Statistically
1041 significant differences are denoted by an asterisk (NS: not significant, $^{**}p < 0.01$, $^{****}p$
1042 < 0.0001 Student's t-test). Data from three independent experimental replicates are
1043 shown (n=5 plants per experiment). Replicates are designated with different colours
1044 (magenta-Replicate 1 (R1), green- Replicate 2 (R2), blue-Replicate 3 (R3)).

1045 **D.** Expression of constructs used for the cell death and conductivity assays in *N.*
1046 *benthamiama* probed by western blot. RGH2-Exo70-FLAG, RGH2^{+}-Exo70-FLAG,
1047 RGH3-HA, the rice blast effector and AVR-Pii^{RbF65E} mutant were detected with the
1048 appropriate antibodies as labelled. Ponceau S staining shows the amount of total
1049 protein loaded per lane in the input.

1050 **E.** As for Fig. 5D but with the AVR-Pii^{Wb} variant and AVR-Pii^{WbF66E} mutant.

1051

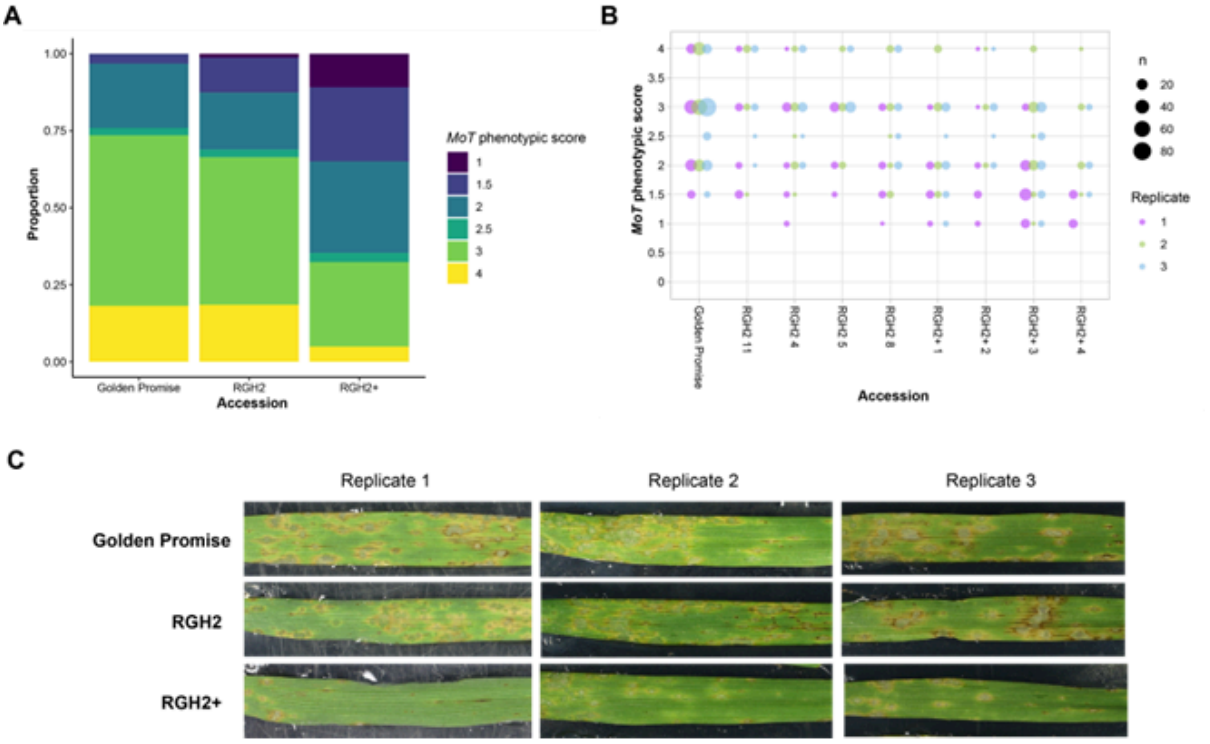

Fig. 6: RGH2⁺/RGH3 transgenic lines show reduced disease severity to *M. oryzae* isolates carrying AVR-Pii^{Wb}.

A. Proportional phenotypes of individuals across Golden Promise control, RGH2, and RGH2+ transgenic lines. Colours indicate ordinal phenotype classes on the 0 – 4 phenotype scale from resistant (0) to susceptible (4).

B. Phenotypic scores from individuals in independent T1 family of RGH2/RGH3 and RGH2+/RGH3 transgenic lines and the Golden Promise control. Phenotypes plotted on the 0 – 4 phenotype scale from resistant (0) to susceptible (4). Circle size indicates the number of individuals with each phenotypic score for each replicate.

C. Macroscopic images of spray inoculations on detached leaves of barley accessions infected with *M. oryzae* isolate Guy11 transformed with AVR-Pii^{Wb}. Representative phenotypes of individuals from T1 families of RGH2/RGH3 and RGH2^{+}/RGH3 transgenics and Golden Promise (the transgenic background) are shown from each experimental replicate.